Development of the Deformation and Primary Recrystallisation Microstructure of an initially Goss-oriented FeSi Single Crystal

Dorothée Dorner, Stefan Zaefferer, Dierk Raabe

Outline

- Introduction
- Experimental techniques
- Deformation texture and microstructure
- Recrystallisation texture and microstructure
- Discussion
- Summary and conclusions
- Outlook

Introduction

Application of silicon steel:

Grain-oriented electrical steel (Fe3%Si)

⇩

iron cores in electrical transformers

Introduction

Application of silicon steel:

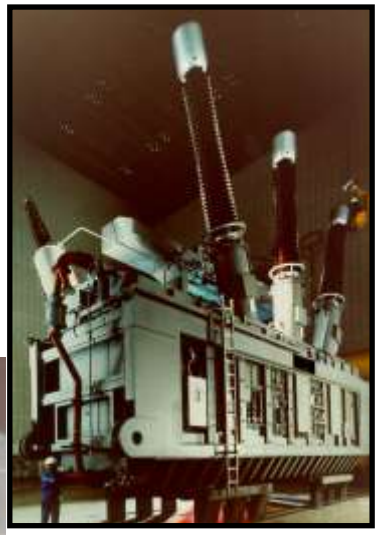

Introduction

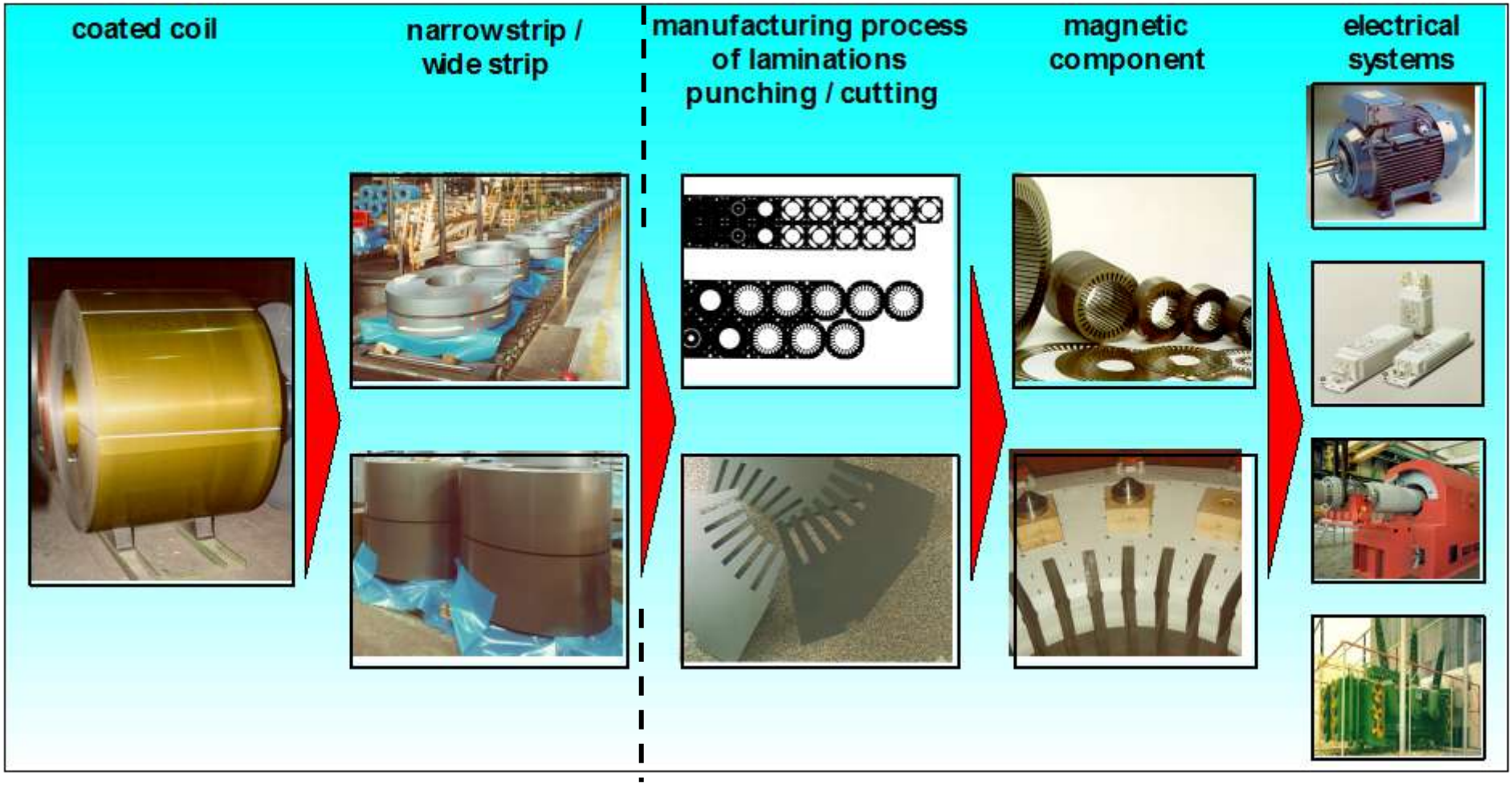

Introduction

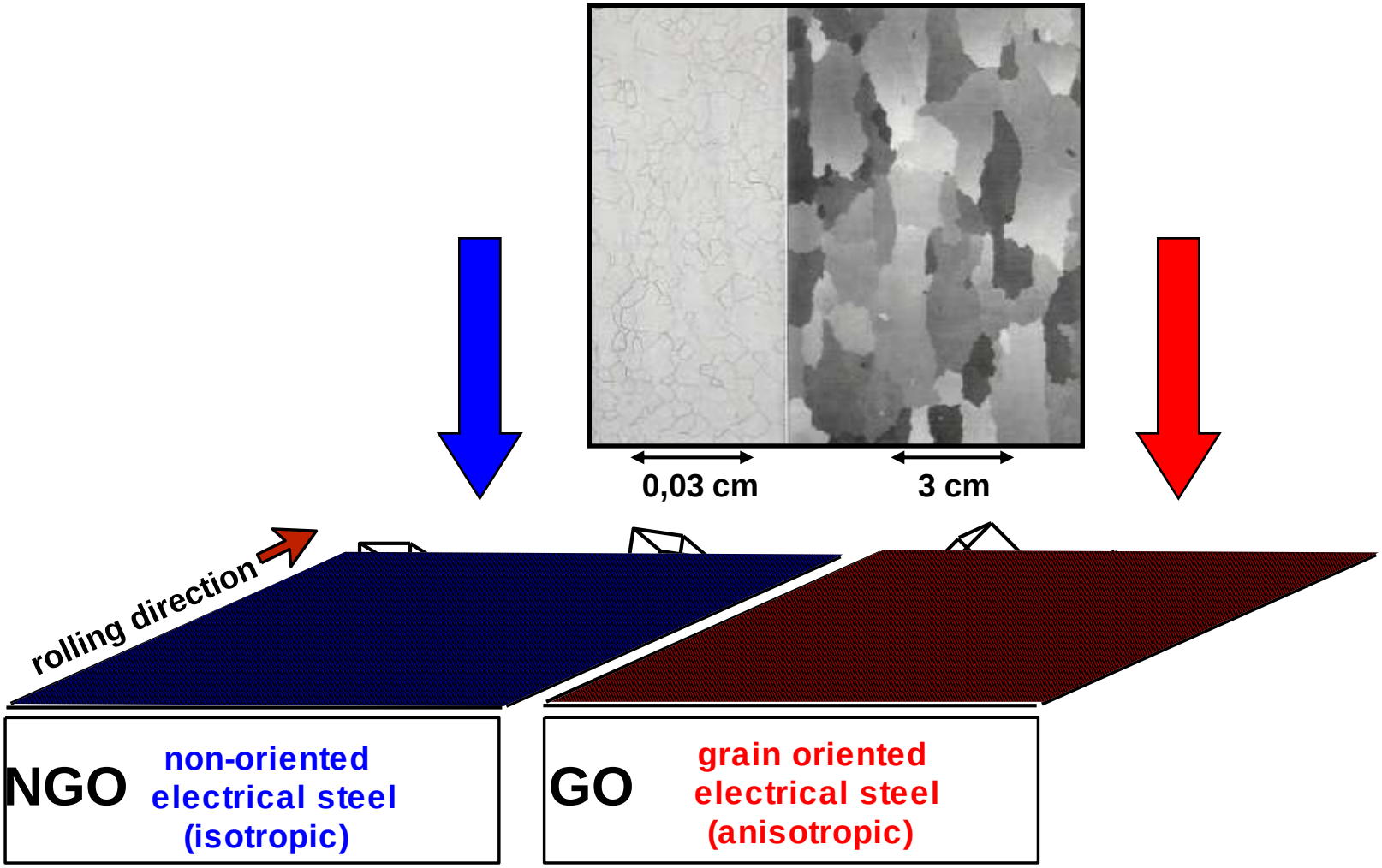

Introduction

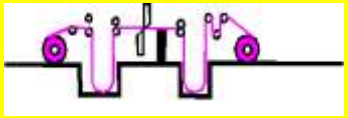

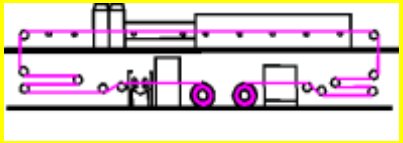

decarb

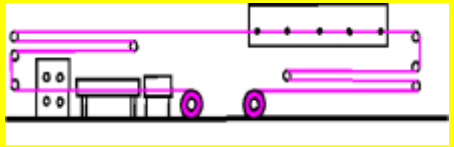

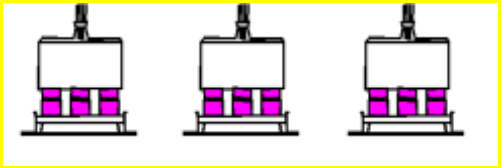

2nd RX

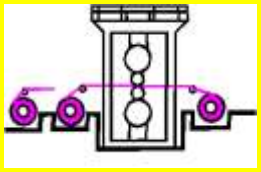

c.r.

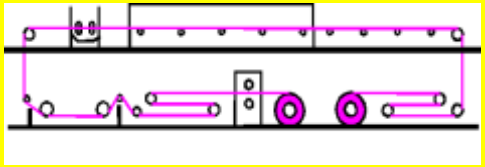

coating

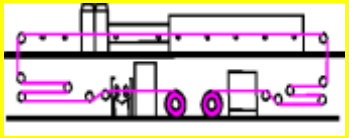

interm. anneal

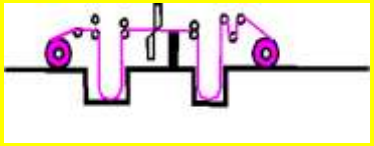

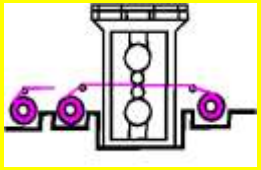

c.r. 2

Introduction

Goss texture in silicon steel:

Easiest directions of magnetisation:
<001>

⇩

{110}<001> preferred orientation
(Goss texture)

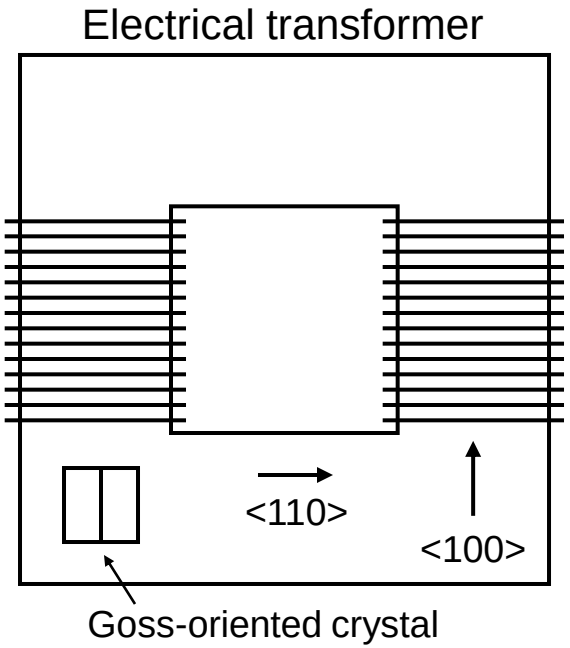

⇨ Secondary recrystallisation of silicon steel:

- abnormal grain growth
- development of sharp Goss texture
- no normal grain growth due to particle inhibition

Introduction

Inheritance of Goss orientation (industrial production cycle):

hot rolling: shear deformation in subsurface layer ⇨ Goss grains

⇩

cold rolling: survival or development of Goss orientation?

⇩

primary anneal: recrystallisation ⇨ minor Goss component

⇩

secondary anneal: abnormal grain growth ⇨ sharp Goss texture

Introduction

Models for abnormal growth of Goss grains:

Possibilities for development of strong texture:

oriented nucleation or growth selection?

Or combination of both?

⇩

currently most favoured:

Σ9 coincidence site lattice model

Introduction

Σ9 coincidence site lattice model:

1) Goss grains ⇨ higher frequency of Σ9 grain boundaries
2) Assumption: Σ9 grain boundaries have a higher mobility

⇩

preferential growth of Goss grains (growth selection)

But:

- sharpness of final texture
- abnormal growth of other orientations
- boundaries mobil in both directions
  ⇨ size advantage of Goss grains?
  ⇨ oriented nucleation of Goss grains?

Introduction

⇨ **Aim of this study:**

Investigation of the microstructure of primary recrystallised Goss grains

⇨ **Search for evidence for an oriented nucleation mechanism!**

Introduction

Motivation for single crystal experiments:

Abnormal grain growth:

Goss nuclei are infrequent: only 1 grain of 10^6 grains grows

⇨ observation of special microstructural properties of potential nuclei is very difficult

⇩

Single crystal rolling and annealing experiments

⇨ more Goss-oriented grains (potential nuclei?) in the primary recrystallised material

Experimental techniques

Experimetal procedure:

1. Single crystal growing experiments

2. Cold rolling:
   89 % reduction in thickness

3. Primary recrystallisation annealing
   (850 °C, wet H_2 + N_2 atmosphere)

Goss-oriented Fe3%Si single crystal

⇨ Investigation of microstructure and texture with x-ray diffraction and electron backscatter diffraction (EBSD)

Deformation texture and microstructure

Texture evolution during cold rolling:

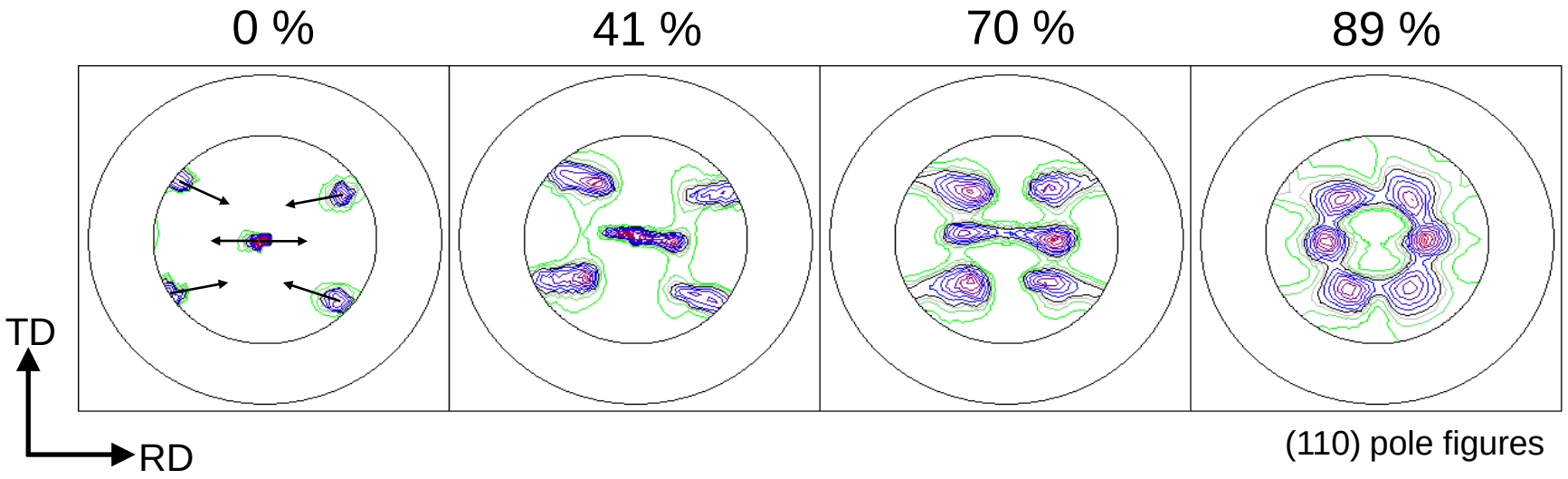

(110) pole figures

rotation of 35° around TD respectively <110> in both directions

Deformation texture and microstructure

Texture of 89 % deformed material:

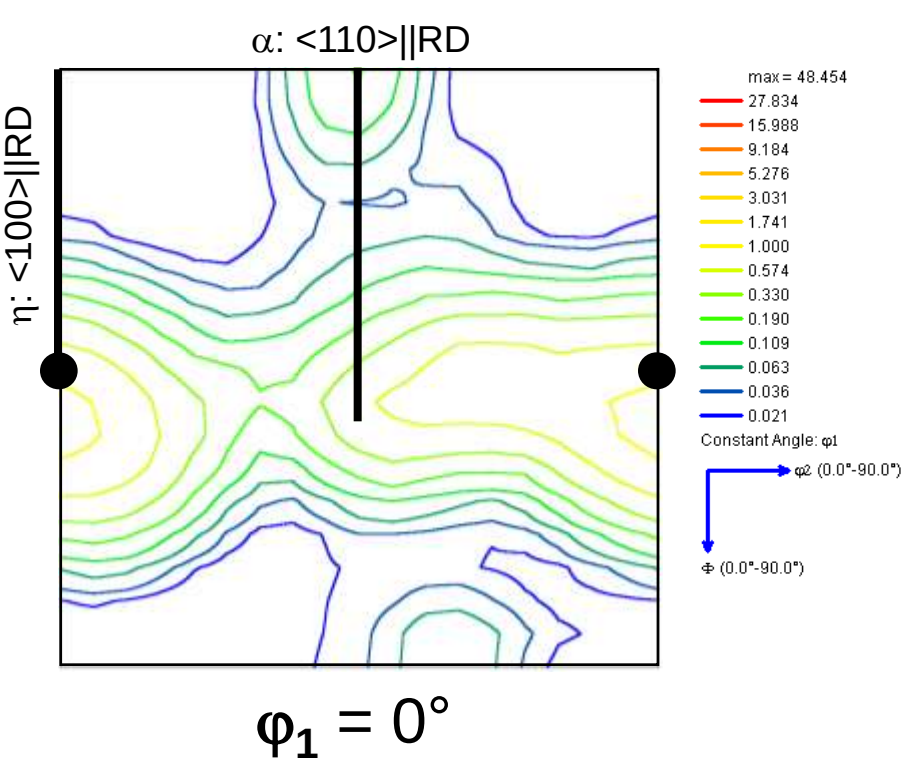

$\varphi_1 = 0°$

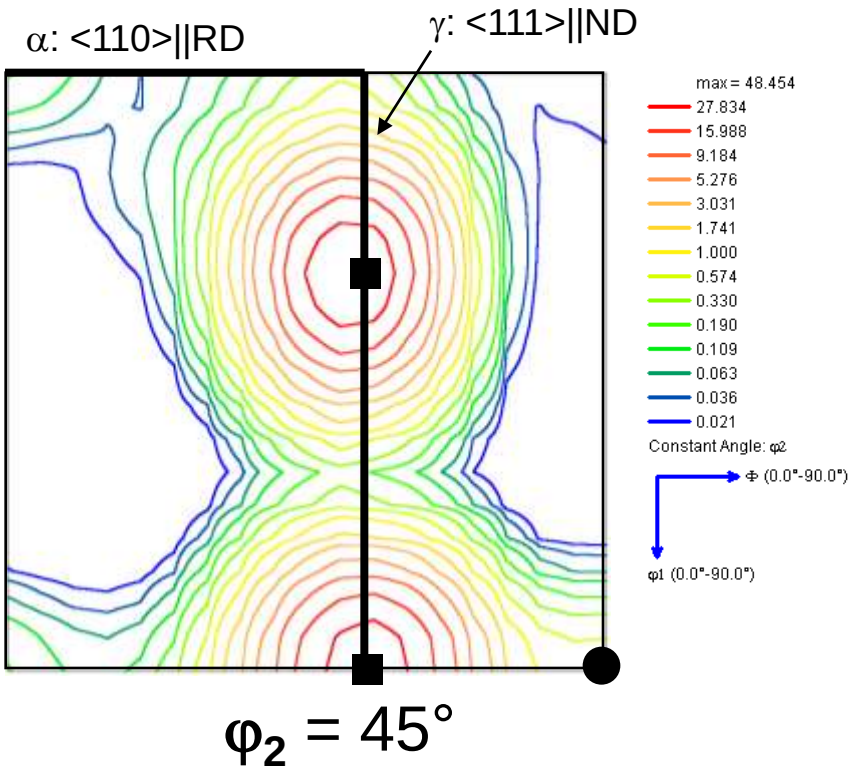

$\varphi_2 = 45°$

● {110}<001> Goss component

■ {111}<112> γ-fibre component

- strong {111}<112> γ-fibre components
- weak Goss component

Deformation texture and microstructure

Evolution of microstructure during cold rolling:

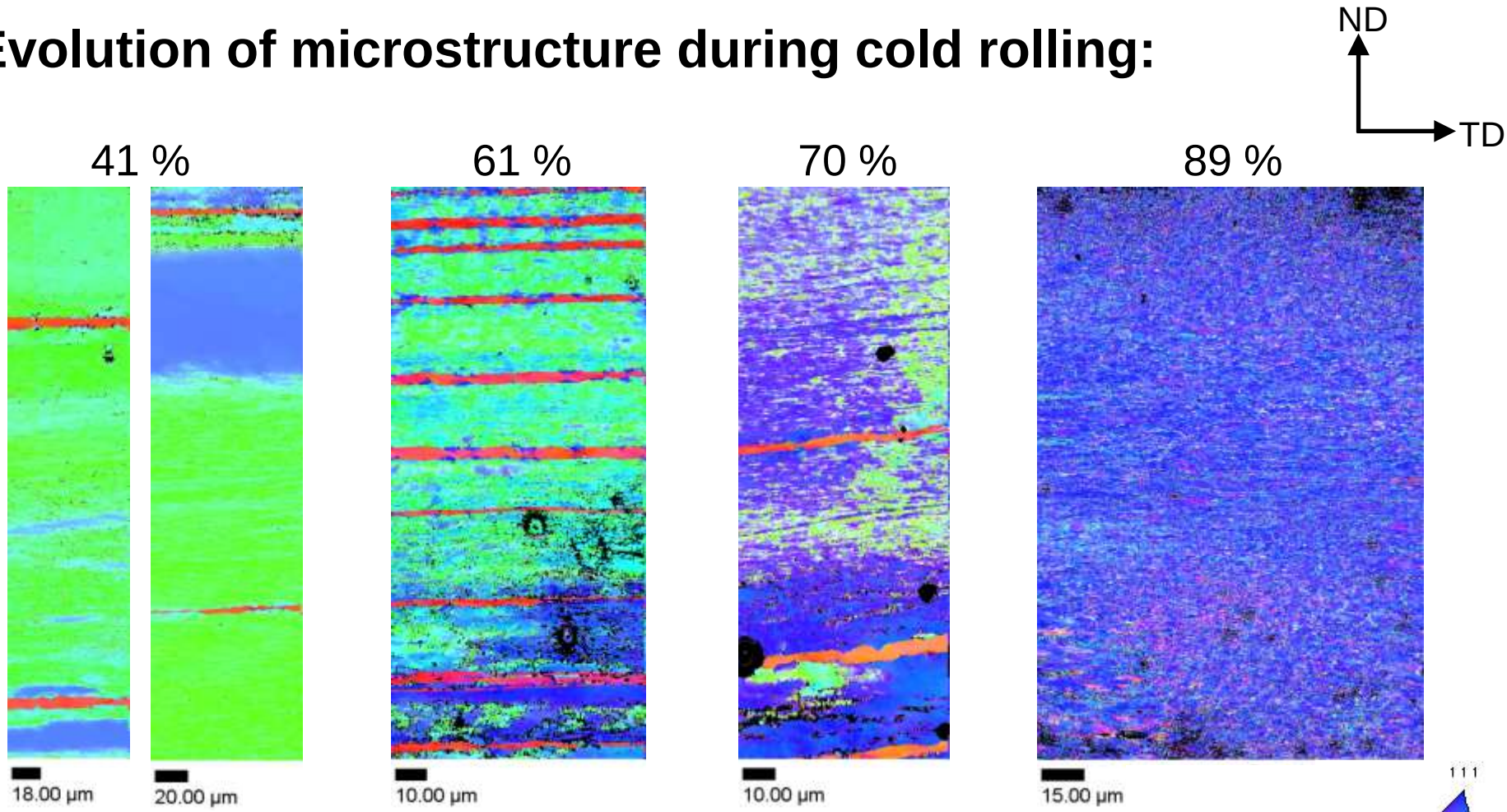

- inhomogeneous deformation
- deformation twins (rotated cube orientation)

Deformation texture and microstructure

Distribution of crystal orientations after 89 % reduction:

transverse section:

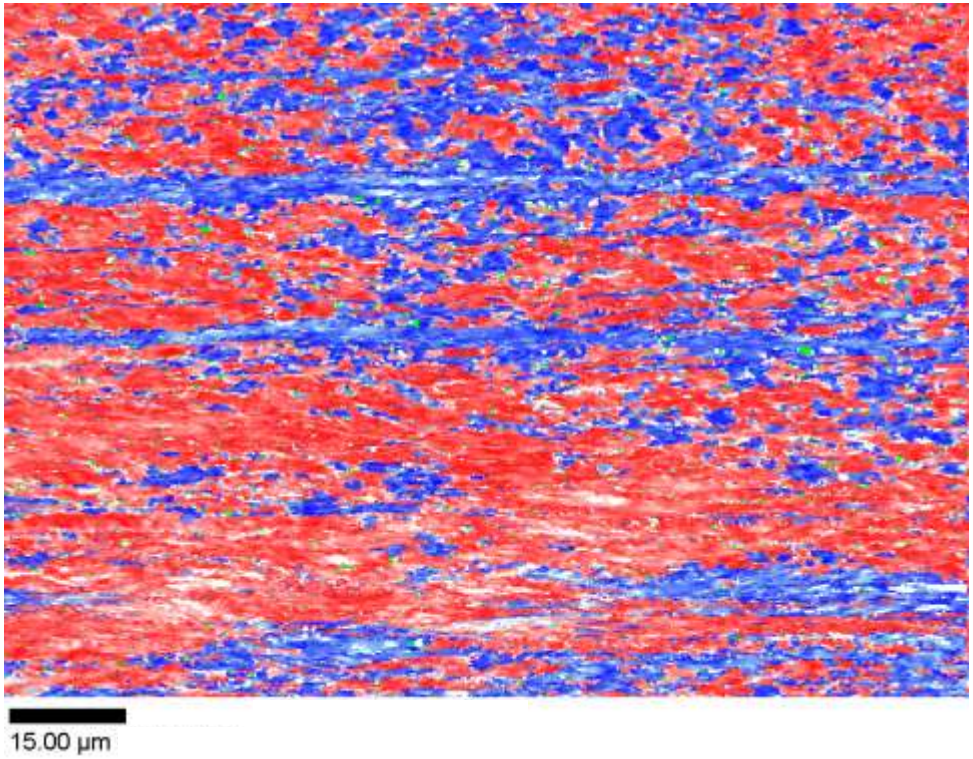

longitudinal section:

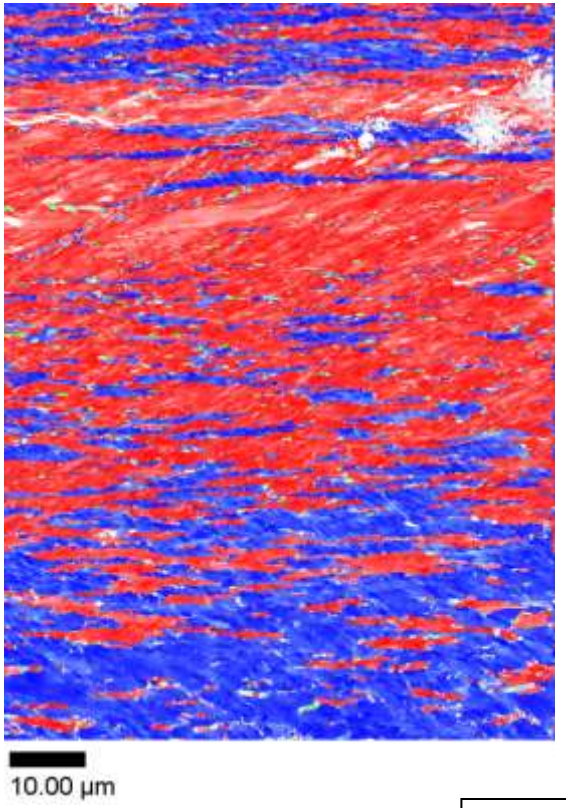

⇨ development of shear bands

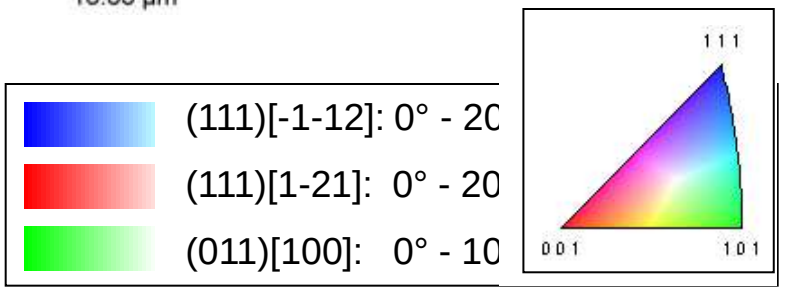

Deformation texture and microstructure

Evolution of Goss-oriented regions during cold rolling:

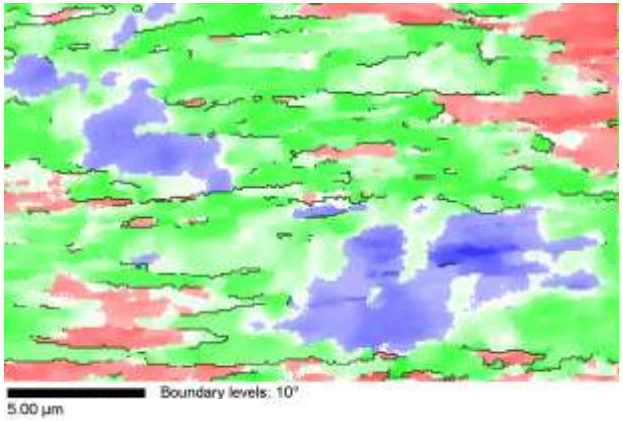

61 %

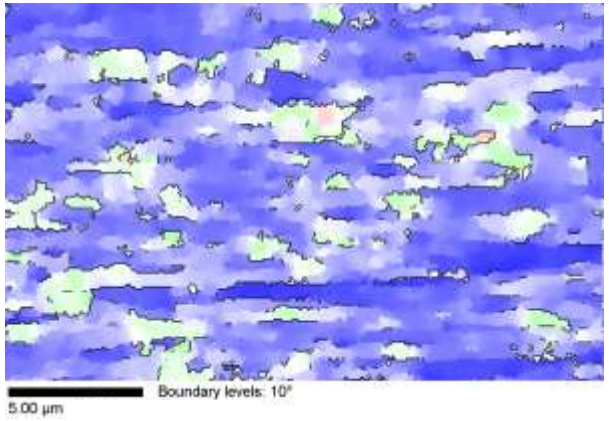

70 %

89 %

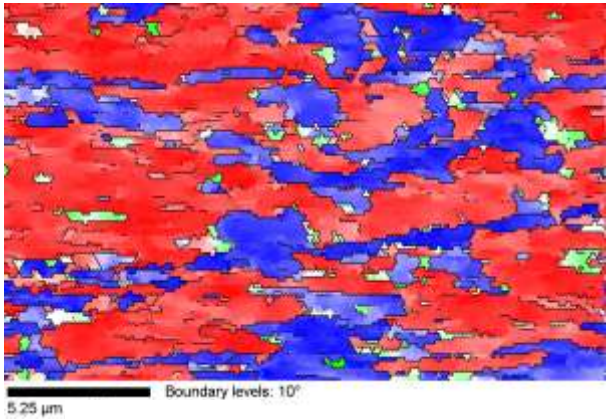

(111)[-1-12]: 0° - 30° misorientation

(111)[1-21]: 0° - 30° misorientation

(011)[100]: 0° - 15° misorientation

- 61%: Goss inside orientation gradients
- 89%: high-angle grain boundaries; orientation gradients within Goss grains

Recrystallisation texture and microstructure

Texture after primary recrystallisation (850 °C, 180 s):

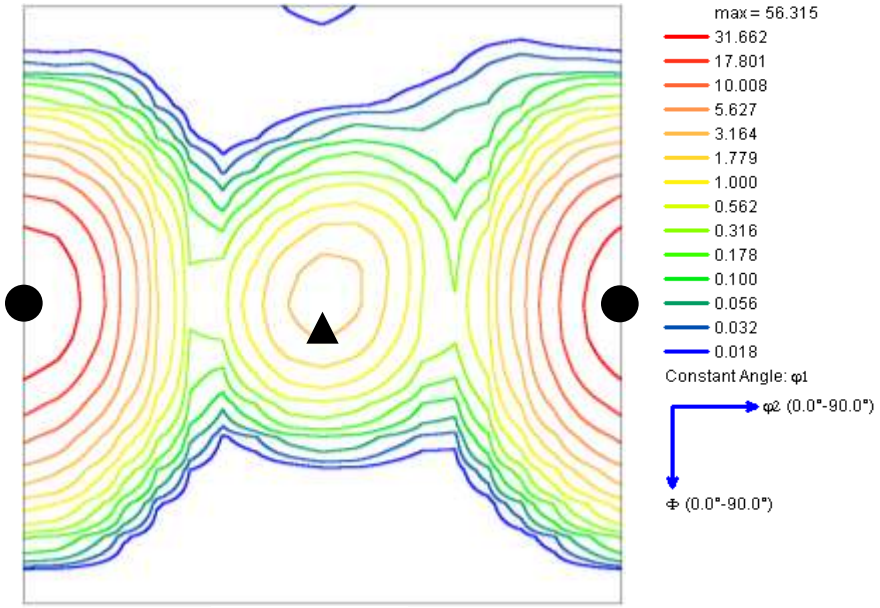

$\varphi_1 = 0°$

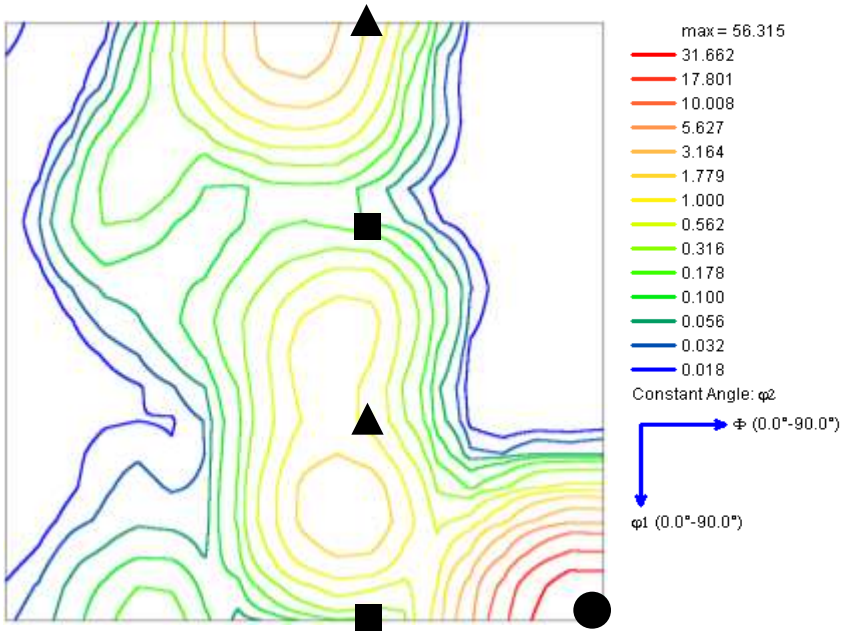

$\varphi_2 = 45°$

- strong Goss texture ⇨ many nuclei for abnormal grain growth?

● {110}<001> Goss component

■ {111}<112> γ-fibre component

▲ {111}<110> γ-fibre component

- recrystallisation of {111}<112> into {111}<110>?

Recrystallisation texture and microstructure

Primary recrystallisation microstructure:

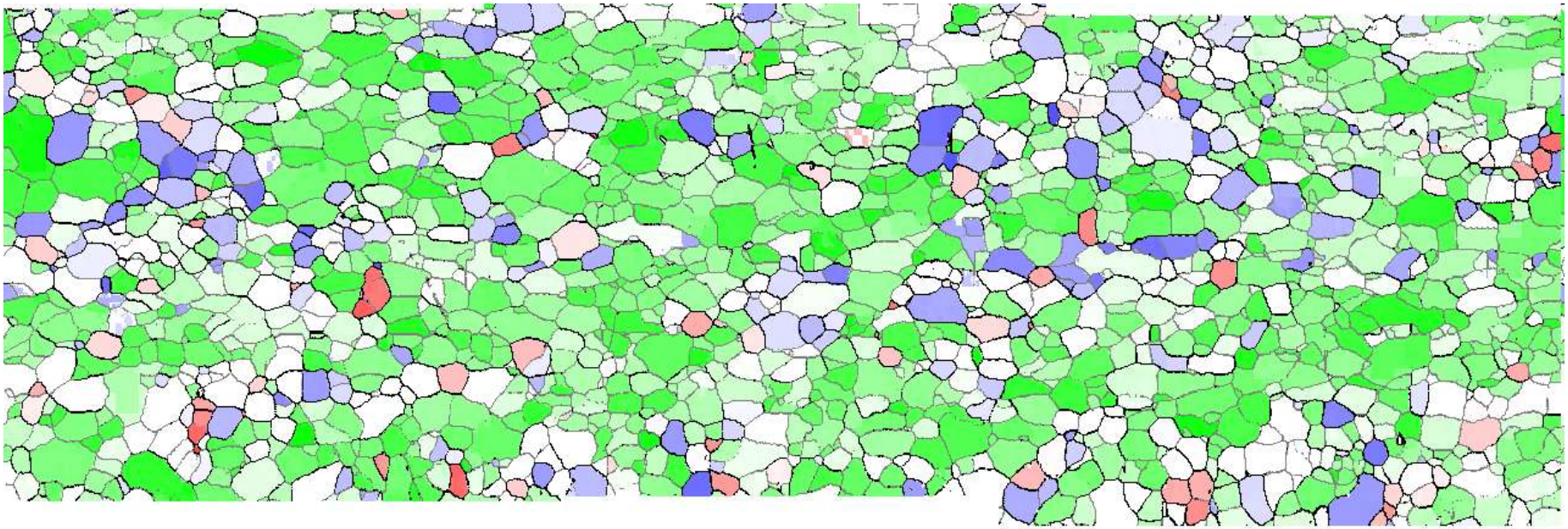

- increase of grain size from 0.3 µm to 13 µm
- 1 of 12 Goss grains recrystallises

Recrystallisation texture and microstructure

Very low angle grain boundaries within Goss grains:

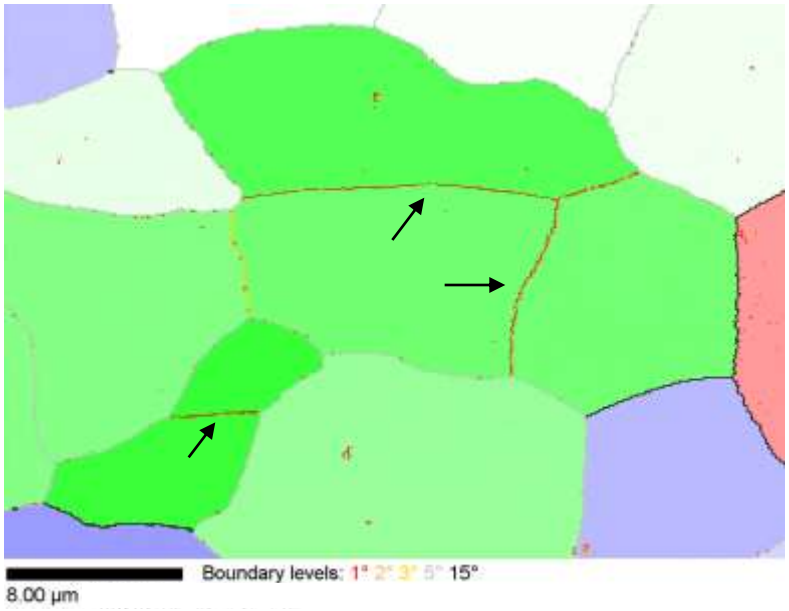

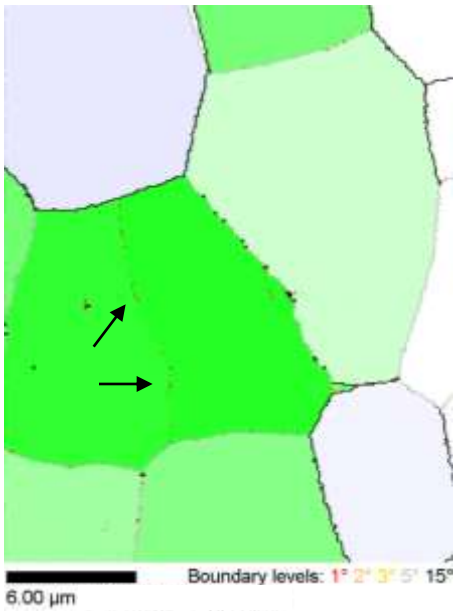

EBSD measurement with high resolution Hough transformation

(111)[-1-12]: 0° - 30° misorientation
(111)[1-21]: 0° - 30° misorientation
(011)[100]: 0° - 15° misorientation

Discussion

Questions:

- Why do Goss-oriented zones survive during cold rolling?
  How do these zones develop?
  How do they form high-angle grain boundaries with the matrix?
- Why do mainly the Goss grains recrystallise during annealing?
- How are the Goss grains internally structured?

Discussion

Development of high-angle grain boundaries:

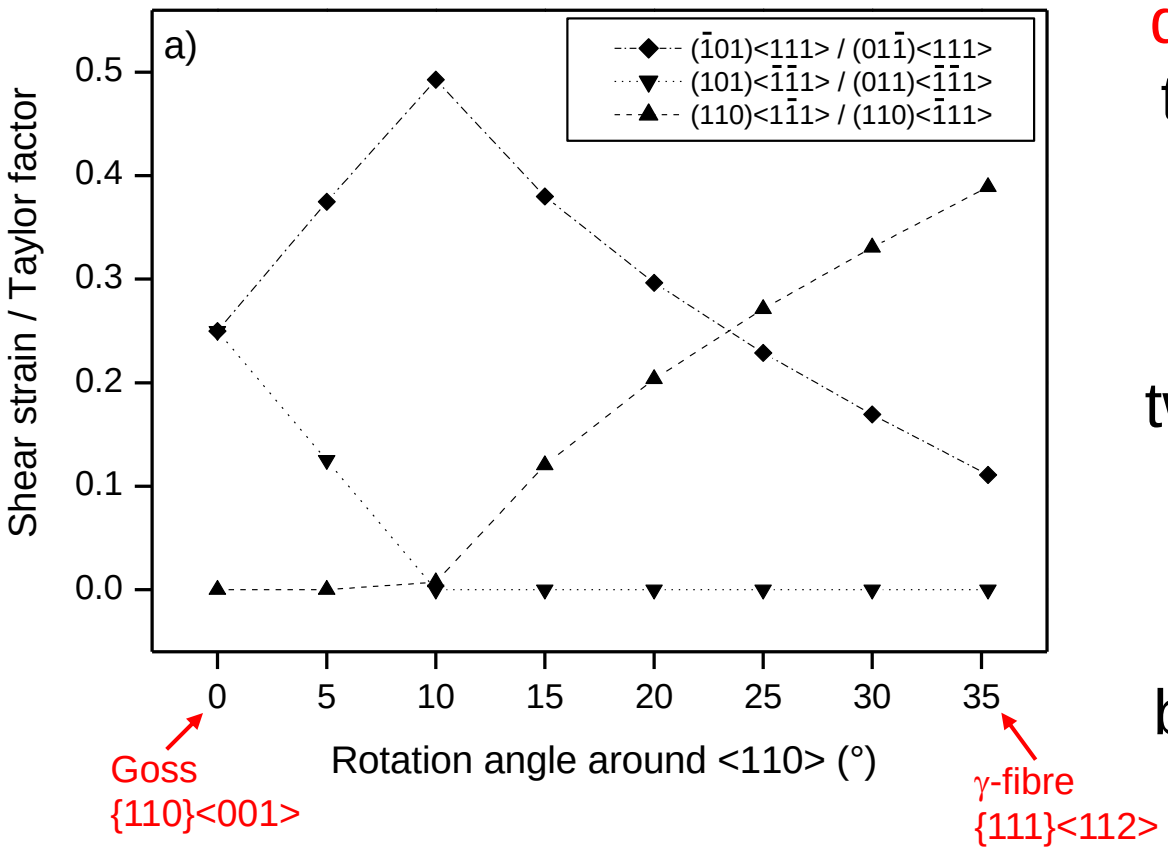

rotation of 10°:
discontinuous transition
to another active set of slip systems

⇩

two adjacent zones with different slip systems

⇩

boundary develops into a high-angle grain boundary

But: Why does Goss remain at all?

Discussion

Nucleation of Goss grains during primary recrystallisation:

- Deformed material: steep orientation gradients
- Recrystallised material: very low angle boundaries

⇩

indicates that nucleation occurs by subgrain growth:

But: How exactly?

Discussion

Growth advantage of Goss grains:

Mobility of grain boundaries:

- Goss grains: high-angle grain boundaries
- γ-fibre components: orientation gradients, low-angle grain boundaries or twin boundaries (geometrical relation)

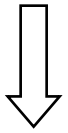

higher mobility of Goss grains

Discussion

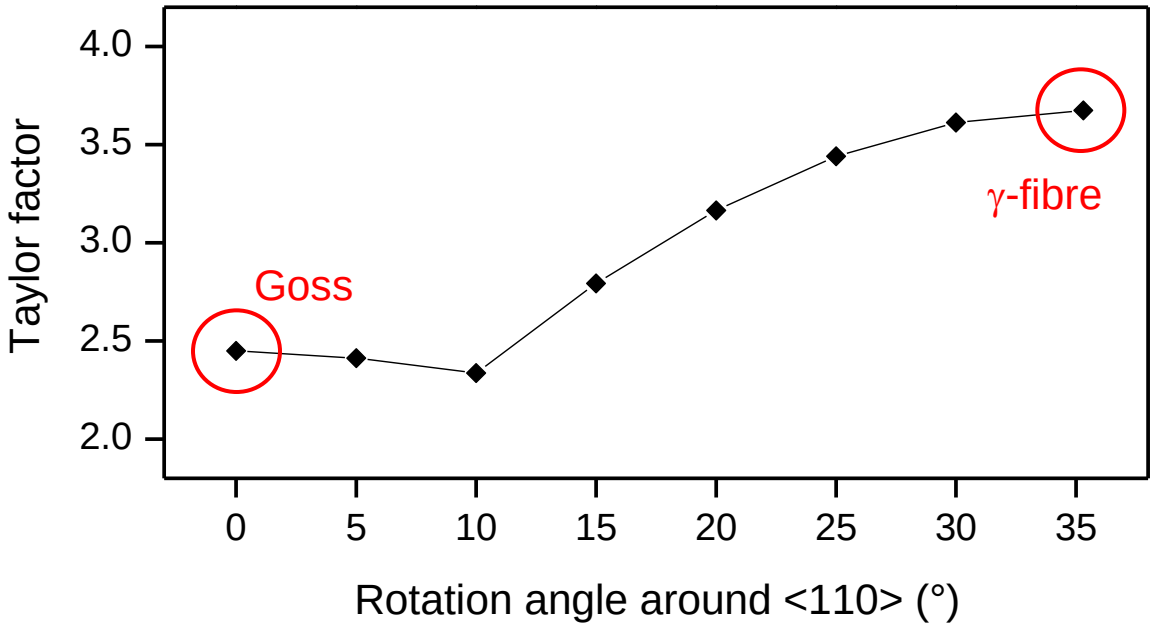

Driving force for recrystallisation:

- lower Taylor factor for Goss
  - ⇨ Goss is easier to deform
  - ⇨ possibly a lower dislocation density for Goss
  - ⇨ difference in stored energies
- (200) Bragg peak half width is smaller for Goss
  - ⇨ lower density of lattice defects

Summary and conclusions

- Cold rolling texture: two major γ-fibre components & minor Goss component ⇨ Goss orientation survives.

- Recrystallisation texture: strong Goss component.

- Left over Goss grains ⇨ nuclei for recrystallisation?

- Orientation gradients in Goss grains after deformation & very low angle grains boundaries in recrystallised Goss grains ⇨ indicate that a special substructure is possibly responsible for preferred nucleation of Goss-oriented grains.

Outlook

single crystal experiments ⇨ many Goss grains
in recrystallised state

⇩

many possible nuclei for abnormal grain growth

⇩

SEM & TEM investigation of substructure within Goss grains

⇩

evidence for an oriented nucleation mechanism for
secondary recrystallisation of Goss grains?

Available online at www.sciencedirect.com
ScienceDirect
Acta Materialia 55 (2007) 2519–2530
Acta MATERIALIA
www.actamat-journals.com

Retention of the Goss orientation between microbands during cold rolling of an Fe3%Si single crystal

Dorothée Dorner, Stefan Zaefferer *, Dierk Raabe

Max-Planck-Institut für Eisenforschung, 40237 Düsseldorf, Germany

Received 13 October 2005; received in revised form 13 November 2006; accepted 18 November 2006
Available online 14 February 2007

Abstract

An FeSi single crystal with an initial {1 1 0}⟨0 0 1⟩ orientation, also referred to as Goss orientation, was cold rolled up to a thickness reduction of 89%. Most of the crystal volume rotated into the two symmetrical {1 1 1}⟨1 1 2⟩ orientations. However, a weak Goss component remained in the highly strained material, even though the Goss orientation is mechanically unstable under plane strain loading. Two types of Goss-oriented regions were discernable in the material subjected to 89% reduction. It appeared that these two types of Goss regions have different origins. Goss grains that were found aligned in shear bands form during straining. A second type of Goss region was found between microbands where the initial Goss orientation was retained.

Keywords: Silicon steel; Goss orientation; Cold rolling; Microband; Shear band

1. Introduction

Silicon steel is a soft magnetic material that is used in electrical power transformers, motors and generators. It has a high silicon content of about 3.2 mass%, which increases the electrical resistivity of iron and, therefore, reduces eddy current losses. Grain-oriented silicon steel that is used for non-rotating applications, i.e. transformers, is characterised by a strong preferred crystallographic orientation. In iron the easiest directions of magnetisation are the ⟨0 0 1⟩ crystal directions. In grain-oriented silicon steel the Goss orientation, i.e. the {1 1 0}⟨0 0 1⟩ orientation[1], is technologically realised to minimise magnetic losses in electrical transformers.

The strong Goss texture of grain-oriented silicon steel is the result of a complex processing scheme, i.e. of a long microstructural and textural inheritance chain. The origin of the evolution of the final Goss orientation is in the hot rolling stage, where the Goss orientation develops below the sheet surface due to shear deformation [1–4]. The particular importance of this Goss-containing subsurface layer was demonstrated by experiments in which the removal of this layer resulted in incomplete secondary recrystallisation [5,1,6]. In the cold rolled material, the fraction of the Goss orientation, considering a misorientation of up to 15°, is about 1% as measured using electron backscatter diffraction (EBSD) [7]. This means that the Goss component is too weak to be detected by X-ray diffraction, as used in earlier studies [e.g. 8,1,9]. In the subsequent primary annealing step, the material recrystallises and the Goss component slightly increases. In the final secondary high-temperature annealing process, normal grain growth is inhibited by particles. However, some of the Goss grains that are present in the recrystallised material grow abnormally. This gives rise to a sharp Goss texture with an average misorientation from the exact Goss orientation of about 3–7°. The exact mechanisms of inheritance of the Goss orientation through

* Corresponding author.
E-mail address: s.zaefferer@mpie.de (S. Zaefferer).

[1] {*h k l*}: Crystallographic plane that is parallel to the sheet plane ⟨*u v w*⟩: crystallographic direction that is parallel to the rolling direction.

1359-6454/$30.00
doi:10.1016/j.actamat.2006.11.048

Available online at www.sciencedirect.com
ScienceDirect
Journal of Magnetism and Magnetic Materials 320 (2008) e657–e660
Journal of magnetism and magnetic materials
www.elsevier.com/locate/jmmm

Texture measurement of grain-oriented electrical steels after secondary recrystallization

M. Frommert[a], C. Zobrist[a], L. Lahn[b], A. Böttcher[b], D. Raabe[a], S. Zaefferer[a,*]

[a]*Max-Planck-Institut für Eisenforschung GmbH, Max-Planck-St. 1, D-40237 Düsseldorf, Germany*
[b]*ThyssenKrupp Electrical Steel, Kurt-Schumacher-St. 95, D-45881 Gelsenkirchen, Germany*

Available online 18 April 2008

Abstract

The measurement of the final Goss texture sharpness in grain-oriented electrical steels is a challenging task due to the immense grain size ranging from millimeters to centimeters. Although, it is widely claimed in the literature that the orientation deviations from the ideal Goss orientation lie in the range of about 7° for conventional grain-oriented steel and in the range of about 3° for high permeability grades, no precise investigation with an appropriate statistical relevance is known to the authors.

In this work, X-ray diffraction and large-area EBSD-based orientation microscopy (EBSD: electron backscatter diffraction) were used for texture analysis and orientation determination in order to estimate the Goss orientation spread of different grades of grain-oriented steel. Two production routes for grain-oriented steel sheets are compared, the conventional route and a low heating route with lower inhibitor strength. The results of the texture measurement demonstrate that both routes deliver comparable values of orientation deviations. Furthermore, it can be shown that small differences of the magnetic properties can be correlated with the texture sharpness of the material.

PACS: 81.40.−z; 81.40.Rs; 75.50.−y; 75.50.Bb

Keywords: Grain-oriented electrical steel; Goss texture sharpness; X-ray diffraction; Electron backscatter diffraction

1. Introduction

Grain-oriented Fe–3% Si steels are used as cores in electrical transformers due to their soft magnetic properties. They are characterized by a sharp $\{0\,1\,1\}\ \langle 1\,0\,0\rangle$ texture (Goss texture) and a very large grain size (in the range of millimeters to centimeters) developing at the end of a complex production process during discontinuous grain growth.

The texture sharpness is usually regarded as a measure of magnetic properties of grain-oriented steels (and vice versa) and misorientations 3° and 7° of the $\langle 1\,0\,0\rangle$ axis from the rolling direction are generally accepted for high permeability (HGO) and conventional grades (CGO), respectively [1–3]. The analysis of the texture sharpness is not at all trivial due to the enormous grain size and it has been a neglected area in the recent years although powerful tools with enhanced measurement speed and precision have been developed.

Increasing quality demands and the pressure to reduce manufacturing costs are the two main driving forces for research and development activities in industry. New production techniques have been recently developed, e.g., low-heating routes and thin-slab-casting methods [4]. Magnetic properties of these materials are of major interest to the steel producers and these properties can be measured with standardized methods. However, little is known about the texture sharpness of the final sheet produced by either of these process routes.

The present paper aims at presenting a couple of methods for measuring the texture of large-grained materials based on X-ray diffraction (XRD) and electron backscatter diffraction (EBSD) in the scanning electron microscope (SEM). In the authors' view, the XRD method has the potential of becoming a standard method for quality control of Goss-textured electrical steel sheets.

*Corresponding author. Tel.: +49 211 6792 803; fax: +49 211 6792 333.
E-mail address: s.zaefferer@mpie.de (S. Zaefferer).

0304-8853/$ - see front matter © 2008 Elsevier B.V. All rights reserved.
doi:10.1016/j.jmmm.2008.04.102

2. Experimental technique

The material used in this investigation was the final sheet of Fe–3% Si grain-oriented steel of two different grades, HGO and CGO. Furthermore, two productions routes were analyzed, the conventional route (route 1) and a low heating route (route 2) with lower inhibitor strength. All the materials were kindly provided by ThyssenKrupp Electrical Steel. In order to check the accuracy of the XRD setup a Goss-oriented Fe–3% Si single crystal, produced at the Max-Planck-Institut für Eisenforschung by zone melting, was also investigated.

XRD measurements were carried out in a goniometer equipped with a sample stage with 6 degrees of freedom: an Eulerian cradle with φ-, χ- and ω-rotations in combination with a translation sample stage with x-, y- and z-movement. At every pole figure measurement position, the sample was moved in x- and y-direction in order to cover a maximum area of the measured sample. For detection, an area detector with a high measurement speed (200 counts/pixel s) was used. The setup further consisted of a cobalt X-ray tube and a collimator for the generation of a parallel beam with 1 mm spot size.

For covering large sample areas, the final sheet was cut by spark erosion into 100 slices of $10 \times 30\,\mathrm{mm}^2$, stacked and mounted in a holder for sample preparation and texture analysis on the cross-section (Fig. 1). With this method, probing of grains from more than $400\,\mathrm{cm}^2$ was realized, containing about 1400 grains in case of CGO (route 1) and about 130 grains in case of HGO (route 1), thus providing excellent statistical data.

XRD analysis was performed using a standard grid of 5° for the φ-rotation, measuring the (1 0 0) and (1 1 0) pole figures which takes a total time of less than 4 h. For determination of the texture sharpness, the peaks of the pole figures were fitted along the φ-circle by a Gaussian distribution: the value of the full-width at half-maximum (FWHM) represents the directional spread about the normal direction and is a measure for the orientation spread of the Goss orientation.

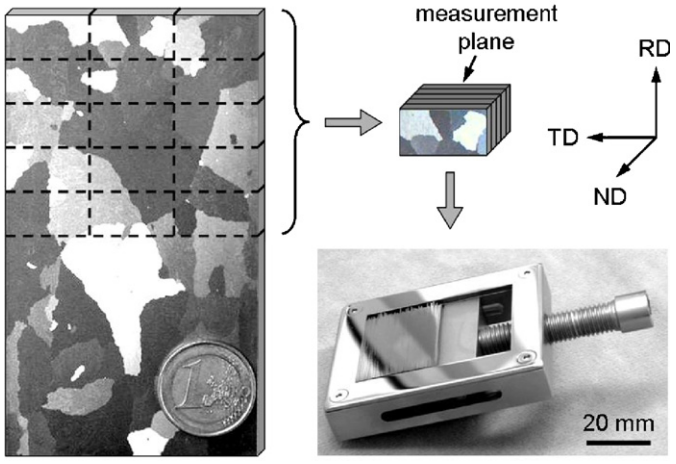

Fig. 1. Sample setup for XRD measurement: a stack of sheets is mounted in a holder for sample preparation and texture measurement on the cross-section.

In contrast to the calculated orientation distribution function (ODF) obtained by X-ray diffraction, the EBSD technique directly *measures* the ODF by means of individual crystal orientation measurements. Therefore, it avoids possible calculation errors. The use of a large-scan EBSD setup enables accurate analysis and rapid acquisition of the diffraction patterns. For the present investigation, a JEOL 840A SEM was utilized. Large-area scans on the sheet surface were realized in a combo scanning mode with a step size of 100 μm, taking about 30 min for a single sample of $2 \times 3\,\mathrm{mm}^2$ size, providing a total area of about $20\,\mathrm{cm}^2$ for the display of the pole figures for each material. It should be mentioned that this area contains only about 70 grains in case of CGO (route 1) and about 10 grains in case of HGO (route 1).

3. Results and discussion

3.1. X-ray diffraction

The pole figures plotted in Fig. 2 show the (1 1 0) poles of CGO (a), of HGO (b), processed by the conventional route 1, and of a Goss-oriented single crystal (c). As expected, the peak width, i.e. the orientation spread, is distinctly larger in the case of CGO material compared to that of HGO. The calculation of FWHM values of the poles in the pole figures delivers orientation spreads of 9° and 6° for CGO and HGO, respectively. These results were obtained with a standard measurement grid of $\Delta\varphi = 5°$. Furthermore, orientation deviations of 11° and 7° were obtained for CGO and HGO, respectively, processed via route 2. All results of the XRD analysis, as summarized in Table 1, show a correlation with the magnetic properties, even in the case of only slight differences with regard to core losses and permeability between the materials of the same grades processed by different routes.

The accuracy of the XRD setup was examined by an additional investigation of a single crystal with exact Goss orientation. For the same measurement grid ($\Delta\varphi = 5°$), an orientation spread of 5°, which matches the magnitude of the grid, was found. A change to higher orientation resolution, i.e. to a smaller grid of $\Delta\varphi = 1°$, led to considerable smaller orientation deviations, in the case of the single crystal to a FWHM value of 1.1° (Fig. 2c). A high-resolution measurement with the narrow grid was accomplished for the HGO material produced via route 1, and a value of 3.8° was found for the orientation spread which is markedly less than the measurement with a larger grid of $\Delta\varphi = 5°$, as shown above. Consequently, for the exact analysis of small orientation deviations a high-orientation resolution, i.e. a fine grid, is necessary, which extends the measurement time by a factor of 3 to 11 h, approximately. However, the total time can be drastically

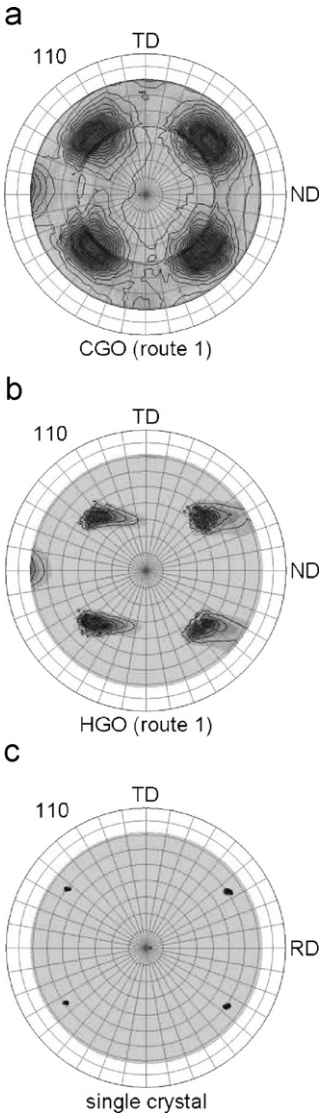

Fig. 2. XRD pole figures of (a) CGO and (b) HGO (both route 1) measured with a grid of $\Delta\varphi = 5^\circ$ and (c) pole figure of a Goss-oriented single crystal measured with $\Delta\varphi = 1^\circ$.

Table 1
Comparison of the texture sharpness measured with XRD and EBSD

Material	Goss orientation spread (deg)			Magnetic properties
	XRD (grid 5°)	XRD (grid 1°)	EBSD	
HGO (route 1)	6	3.8	3.2	high
HGO (route 2)	7	–	3.1	
CGO (route 1)	9	–	5.9	
CGO (route 2)	11	–	5.3	low

reduced (by a factor of 4 or more) if only one peak of the pole figure is measured which is sufficient for the analysis proposed above.

3.2. EBSD measurement

Examples of EBSD measurements obtained from single scans of HGO and CGO samples processed via route 1 are shown in Fig. 3. It is obvious that the grain size of HGO is drastically larger than that of CGO. Furthermore, the orientation deviation from the ideal Goss orientation is less in the case of HGO as can be seen from the coloring of the mappings.

In order to account for the inaccuracies due to sample positioning and minor statistical aberrations, the texture sharpness was not directly calculated as the deviation from the theoretical Goss orientation. Instead, a reference orientation well out of the Goss orientation spread was

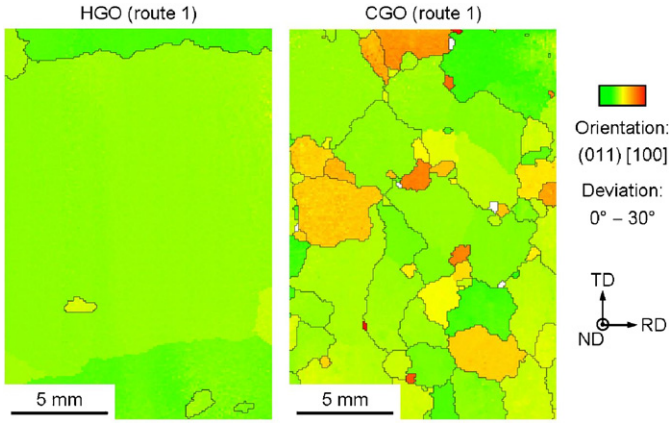

Fig. 3. EBSD images of the normal plane of HGO and CGO (both route 1); the color code indicates the deviation from the ideal Goss orientation.

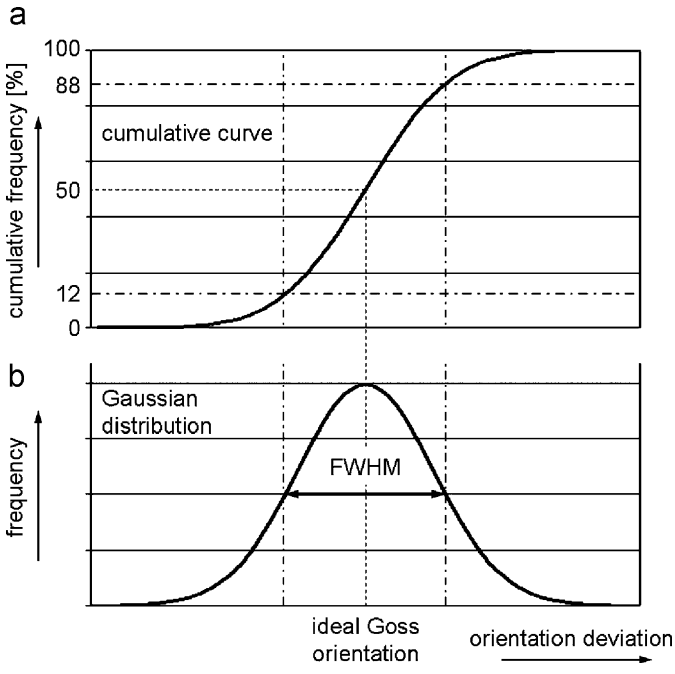

Fig. 4. Schematic diagram of the cumulative frequency of the deviation from the ideal Goss orientation and resulting Gauss distribution used for the evaluation of the EBSD data.

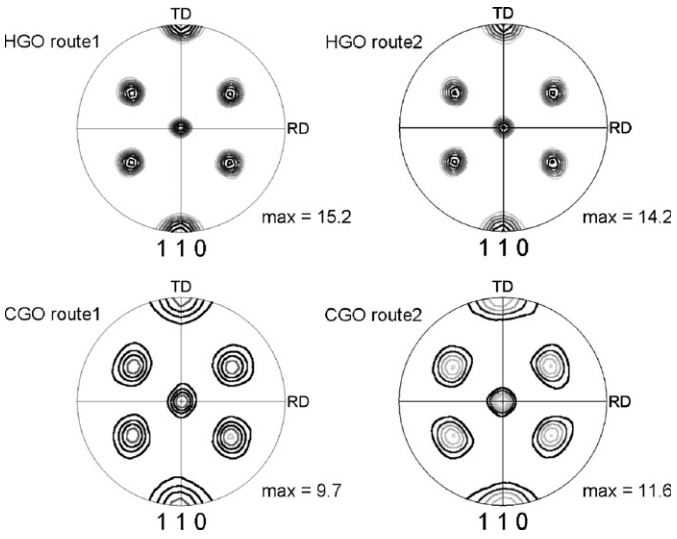

Fig. 5. EBSD pole figures of HGO and CGO for routes 1 and 2.

selected and the deviation from this theoretical orientation was measured and classified into intervals of 1°. From these data the cumulative frequency was calculated, shown in Fig. 4a. Subsequently, an orientation distribution was computed from the cumulative curves under the following assumptions:

1. The true major orientation is the Goss orientation.
2. The deviation from the ideal Goss orientation follows a Gaussian distribution.

The appropriate distribution is shown in Fig. 4b. The FWHM values determined from these curves are collected in Table 1. The texture sharpness tends to have smaller values—about 3° for HGO and 6° for CGO—compared to the XRD results measured with $\Delta\varphi = 5°$. The same tendency is found concerning the difference between the two grades of electrical steel. Moreover, the result the high-resolution XRD analysis ($\Delta\varphi = 1°$) performed with HGO (route 1) is in good agreement with the result of the EBSD measurement.

For a better visualization, Fig. 5 displays the (1 1 0) pole figures for both grades of the material processed via routes 1 and 2. The texture data were obtained from the EBSD measurements after merging all the maps belonging to one sample. A comparison of the pole figures shows larger orientation spreads and lower intensities for CGO compare to those for HGO, but shows similar peak width for the same material processed via routes 1 and 2.

4. Conclusions

Both measurement techniques, X-ray diffraction and EBSD, deliver comparable values for the Goss orientation spreads and they lie in the range of about 3° for HGO and about 6° for CGO. Furthermore, it is shown that both production routes—the conventional and the low heating process—deliver materials of comparable texture sharpness. The setup proposed for X-ray measurement offers an efficient tool for the determination of the texture sharpness of large-grained materials due to excellent statistics and less experimental effort compared to EBSD measurements. The measurement time for the XRD analysis can be drastically reduced if only one peak of the pole figure is measured, which is sufficient for determination of texture sharpness.

Further experiments are currently being performed to complete the XRD measurements with high orientation resolution ($\Delta\varphi = 1°$) in order to further correlate the texture sharpness with magnetic properties of materials processed by different production routes.

References

[1] R. Ricci Bitti, M. Candiotti, J. Magn. Magn. Mater. 26 (1982) 11.
[2] S. Mishra, et al., Acta Metall. 12 (1984) 2185.
[3] M. Matsuo, ISIJ Int. 29 (1989) 809.
[4] K. Günther, et al., Steel Res. Int. 76 (2005) 413.

the process chain and details of abnormal Goss grain growth in the secondary annealing stage are still unclear [10].

The investigation of the microstructural evolution of the Goss orientation from the hot rolling stage to the final secondary recrystallisation in the industrially processed material is difficult, since Goss grains are very rare both in the cold rolled and the primary recrystallised state. However, in an early study Dunn [11] observed that, after deformation and primary recrystallisation of an initially Goss-oriented single crystal, the volume fraction of Goss grains is higher than in the industrially processed polycrystalline material. Moreover, Mishra et al. [1] pointed out that the large Goss grains that are present in the subsurface layer of hot rolled silicon steel (Fig. 1) and which are essential for the development of the final Goss texture, qualitatively behave like Goss-oriented single crystals. Therefore, in this study a Goss-oriented single crystal was used as the starting material for the cold rolling and annealing experiments (Fig. 1). Such model experiments allow a detailed investigation of Goss grains in the deformed state and therefore might lead to an improved understanding of the incipient state of primary recrystallisation. Furthermore, Goss grains in the primary recrystallised state, which provide the nuclei for secondary recrystallisation, specifically for abnormal Goss grain growth, can be characterised in detail. One particular question in this context is whether these grains have particular properties that allow them to grow abnormally.

This publication exclusively focuses on the evolution of the microstructure and microtexture of the initially Goss-oriented FeSi single crystal during cold rolling. The results of the investigations on the primary recrystallised material will be presented in a forthcoming study. A detailed investigation of the microstructure evolution during cold rolling, with the aid of high-resolution EBSD, revealed that two types of Goss-oriented regions were present in the deformed material. These two types were related to either shear bands or microbands. These new findings particularly raised the following questions: (1) How is some fraction of the starting single crystal Goss orientation retained during cold rolling, even though it is mechanically unstable in body-centred cubic (bcc) metals upon plane strain deformation [12,13]? Or does it disappear and reform during rolling deformation? (2) What are the roles of shear bands and microbands during rolling deformation, in particular for the stabilisation of the Goss orientation?

2. Experimental procedure

The starting material for this study was an industrially hot rolled silicon steel strip with 3.24 mass% Si and MnS as an inhibitor, which is employed for the production of conventional grain-oriented (CGO) electrical steel. This material was used to grow a single crystal with $\{1\,1\,0\}\langle 0\,0\,1\rangle$ orientation using the Bridgeman method. First, the sample was connected to a Goss-oriented seed crystal. Then the sample and a part of the seed crystal were melted and subsequently solidified starting from the seed crystal. This resulted in a single crystal sample with the orientation of the seed crystal (Fig. 2). The as-grown single crystal was almost perfect, containing only a very small number of low-angle grain boundaries with misorientations of about 1°. The single crystal was machined to a thickness of 2.20 mm, which is about the thickness of a industrial hot rolled strip, a width of 21 mm and a length of about 55 mm. This strip was cold rolled without lubrication in a laboratory rolling mill with a roll diameter of 105 mm, a rolling velocity of 10 m/min and a load of 120 kN. In 14 passes the sample was rolled to a thickness of 0.25 mm corresponding to a total engineering thickness reduction of $\varepsilon = 89\%$ (true logarithmic strain of $\varphi = 2.2$).

The texture and microstructure of the deformed samples were investigated using electron diffraction techniques both in a scanning electron microscope (SEM) and in a transmission electron microscope (TEM). EBSD measurements were carried out using a field emission gun SEM (JEOL JSM 6500F). The software OIM (EDAX/TSL) was used to index the Kikuchi diagrams and for the evaluation of the orientation data. Microtexture measurements were also done by TEM and the Kikuchi patterns were indexed using the software Toca [14].

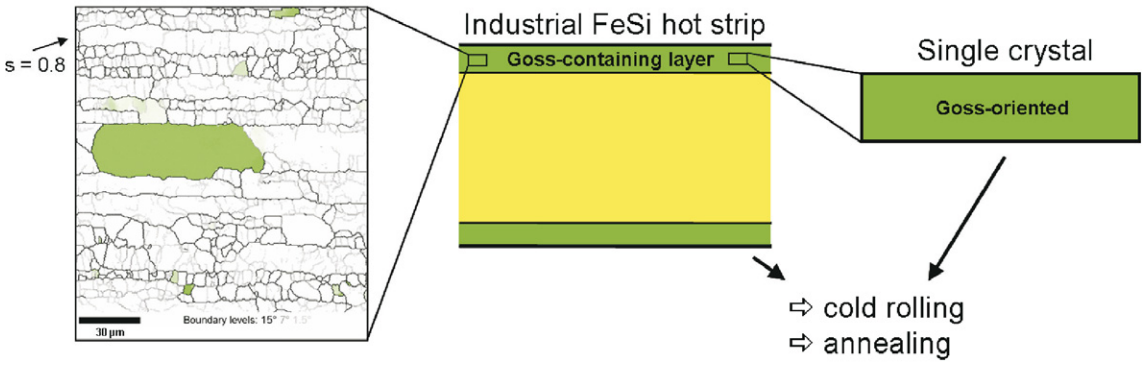

Fig. 1. Goss grain in an industrial FeSi hot strip (left) and the idea of the single crystal experiments (right).

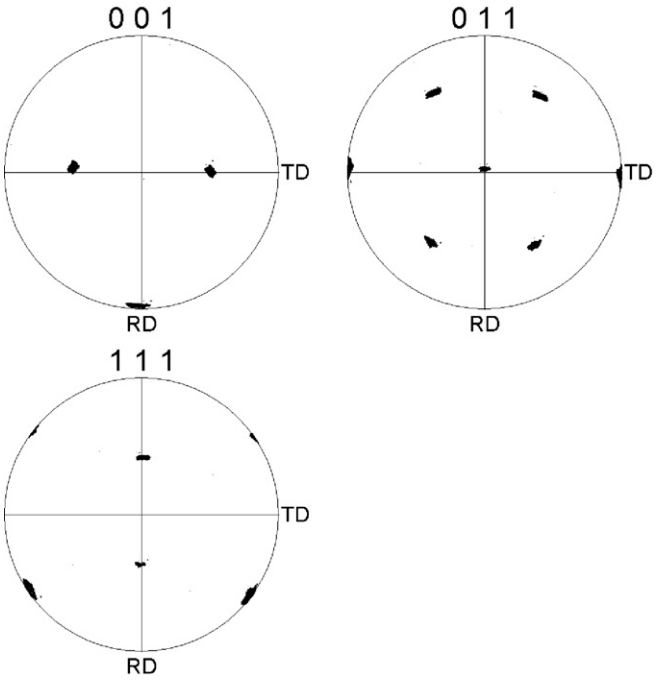

Fig. 2. Orientation of single crystal before cold rolling. Pole figures obtained from EBSD measurements.

3. Results

3.1. Texture and microstructure evolution during cold rolling

Both X-ray and EBSD data showed that in the course of cold rolling most of the initially Goss-oriented single crystal rotated in two opposing directions to the two symmetrically equivalent $\{1\,1\,1\}\langle 1\,1\,2\rangle$ orientations. This rotation amounted to 35° around the $\langle 1\,1\,0\rangle$ crystal direction, which is parallel to the transverse sheet direction (TD). In contrast to earlier studies using X-ray diffraction (e.g. [11]), not only the two strong $\{1\,1\,1\}\langle 1\,1\,2\rangle$ texture components were observed (Fig. 3a), but the EBSD data revealed that even after highest deformation of 89% a weak Goss component was present (Fig. 3b).

The evolution of the microstructure and microtexture during cold rolling was studied by EBSD. At low thickness reductions, the spatial distribution of the Goss and the $\{1\,1\,1\}\langle 1\,1\,2\rangle$ texture components was quite inhomogeneous throughout the deformed sheet (Fig. 4). However, in the 89% deformed material the texture in the sheet center and in the region close to the sheet surface were very similar. This indicated that there was no pronounced effect of shear stress due to friction at the sheet surface.

Characteristic microstructural features were microbands and at higher strain microscopic shear bands, which are described in more detail below. Furthermore, mechanical twinning (first order twins) occurred. The twinning planes of the $\{1\,0\,0\}\langle 0\,1\,1\rangle$-oriented twins were parallel to the transverse direction and inclined by about 10° to the rolling direction (RD). The volume of these deformation twins increased during deformation up to 61% thickness reduction and decreased at higher strain.

3.2. Occurrence of microbands and shear bands

EBSD and TEM investigations revealed that microbands frequently form during cold rolling of the Goss-oriented single crystal (Figs. 5 and 6). *Open microband* denotes a microstructural feature that is characterised by two straight, closely spaced dense dislocation walls enclosing a small elongated volume [15]. A *closed microband* is an elongated, straight dense dislocation wall that often occurs in groups of parallel bands. In this study the misorientation across a single wall was about 10° or higher and the sense of rotation was opposite on two successive walls (Fig. 7).

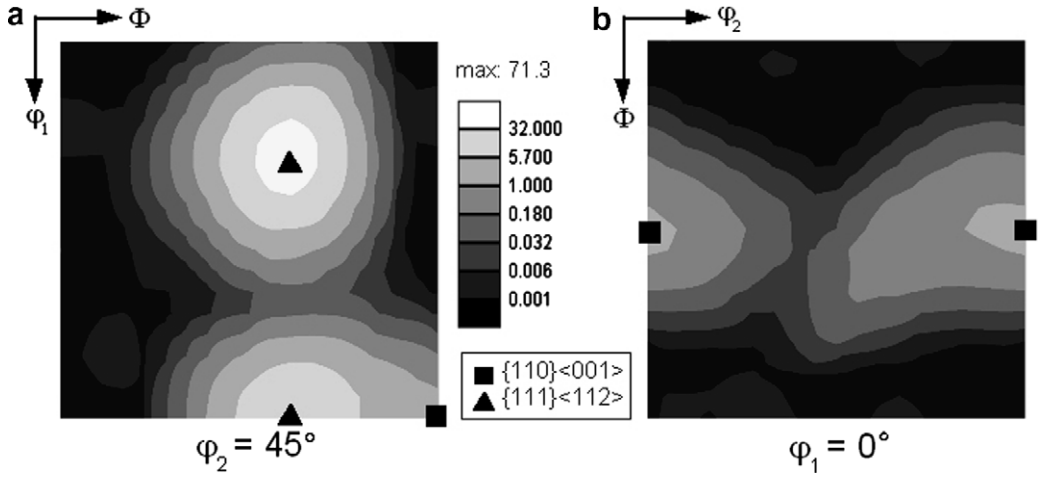

Fig. 3. Texture of the 89% deformed, initially Goss-oriented material. Orientation distribution function of EBSD data displayed in a $\varphi_2 = 45°$ section (Bunge notation) (a) and a $\varphi_1 = 0°$ section (b) through the Euler space. The texture components with the highest intensities are the two symmetrically equivalent $\{1\,1\,1\}\langle 1\,1\,2\rangle$ components (a). In addition, a weak Goss component is observed, with a texture intensity of about 1 (b). Note that the texture intensity scale is logarithmic.

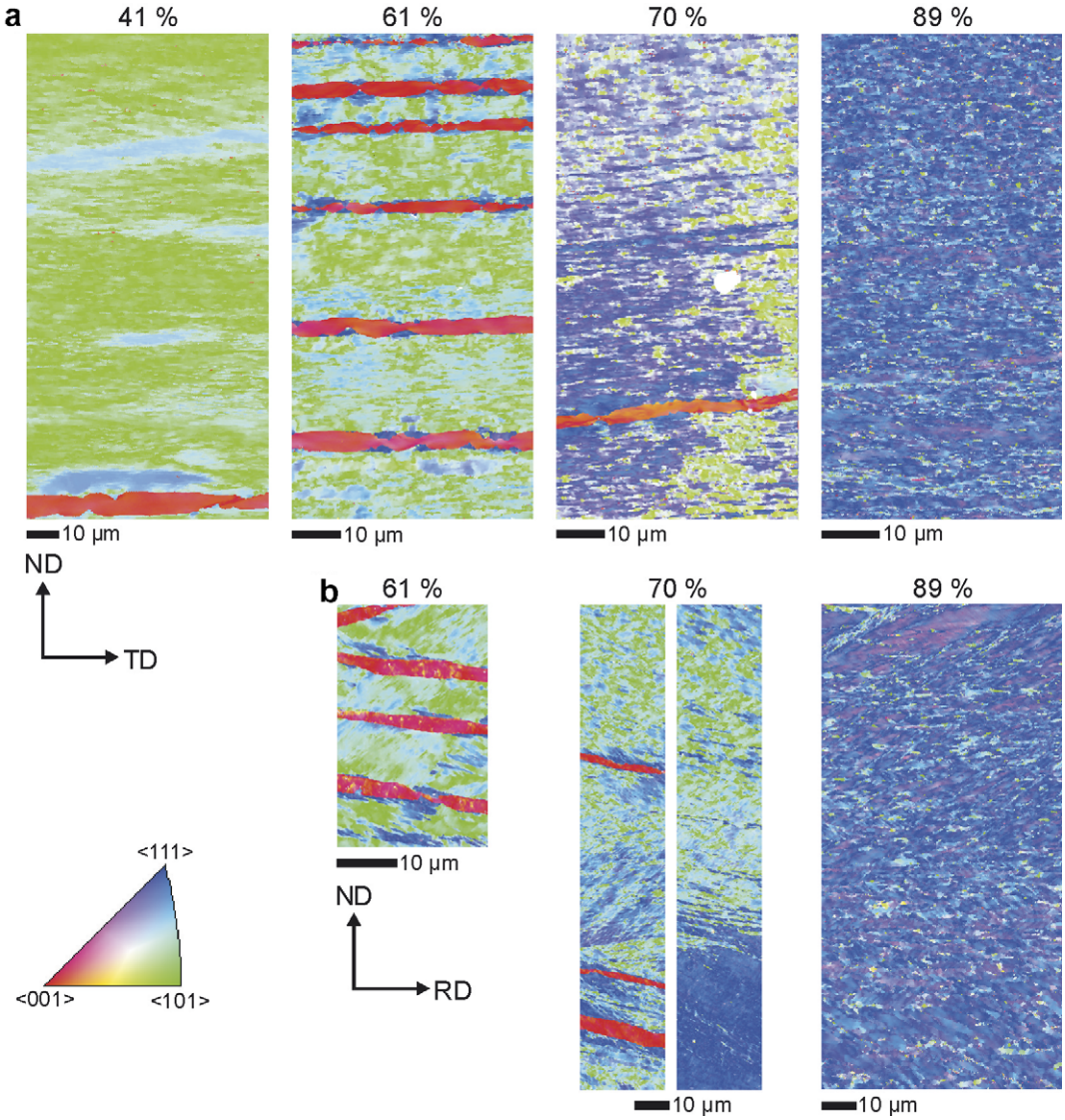

Fig. 4. Evolution of the microstructure during cold rolling of an initially Goss-oriented single crystal. Inverse pole figure maps for the normal sample direction as obtained by EBSD for samples with a thickness reduction of 41% ($\varphi = 0.5$), 61% ($\varphi = 1.0$), 70% ($\varphi = 1.2$) and 89% ($\varphi = 2.2$), respectively: (a) ND–TD sections; (b) ND–RD sections. ND: normal direction; RD: rolling direction; TD: transverse direction.

Therefore, the misorientation across a closed microband, which consists of two walls of opposite rotation, was very small. These observations were consistent with those of Chen et al. [15], although they observed a smaller misorientation. This difference might be attributed to the fact that they investigated less strained material.

At a strain of 55%, in some areas microbands started to form (Fig. 8), while in other areas they were already well developed (Fig. 6), indicating that deformation is inhomogeneous at lower strain. Fig. 8 shows an area with a microstructure characterised by two crossing sets of linear features with inclination with respect to the rolling direction of about 46° and 34° or less. Possibly this reflects an early stage of microband development, and presumably, during further deformation, these two sets would develop into the characteristic microstructure with parallel microbands (Figs. 5 and 6). The parallel microbands were with about 22° less inclined (Fig. 6). Analysis of the orientation of the microbands with respect to the adjacent crystal orientation in both ND–TD sections and ND–RD sections (ND: normal direction) showed that the microband habit planes are close to {1 1 2} crystal planes, but not related to {1 1 0} planes. At 55% strain, many microbands comprised both open and closed parts (Fig. 7). At higher strain, the number of open microbands decreased and at the highest reduction of 89% all the microbands were closed. The inclination of the microbands decreased during straining until they were at the highest reduction roughly parallel to the rolling direction. At high strain of 89% thickness reduction, the microbands were still discernible in the deformed microstructure, but they occurred together with microscopic shear bands.

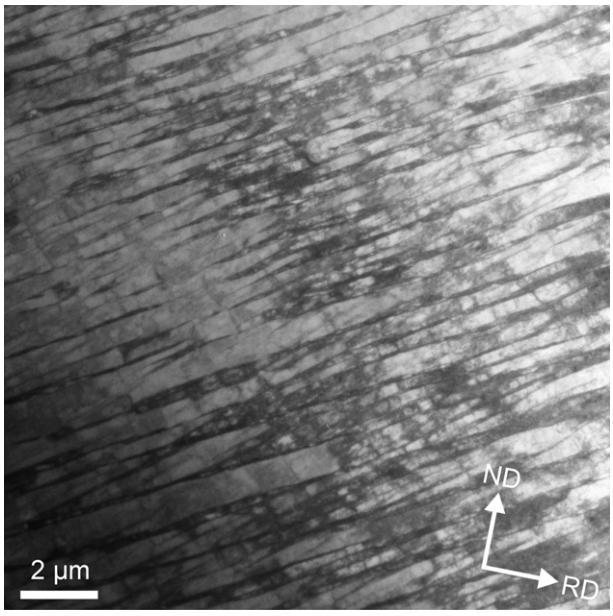

Fig. 5. Microbands in a 55% deformed, initially Goss-oriented single crystal. TEM bright field image.

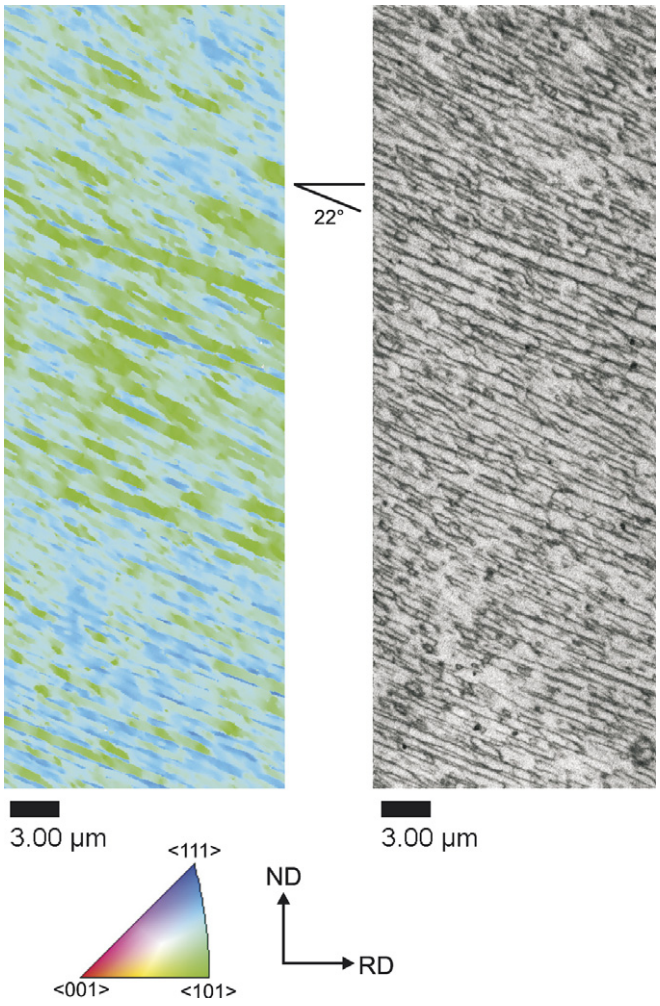

Fig. 6. Region with well-developed parallel microbands in a 55% deformed, initially Goss-oriented FeSi single crystal. The inclination of the microbands to RD is indicated. (a) Inverse pole figure map for the normal sample direction as obtained by EBSD. (b) EBSD pattern quality map showing microbands as linear features with low EBSD pattern qualities.

Microscopic shear bands formed in cold rolled samples with thickness reductions of 77% ($\varphi = 1.5$) and higher [16]. They can be clearly recognized in EBSD pattern quality maps as linear features with a poor pattern quality (Figs. 9 and 10). The EBSD pattern quality generally becomes worse with increasing crystal lattice distortions due to a high dislocation density. The observed shear bands sheared the deformation twins, which developed at a lower strain. This observation was used to estimate the corresponding local shear strain to about 2. When viewed on ND–RD cross-sections, the shear bands were initially inclined by 29–36° to the rolling direction, with smaller inclination angles additionally occurring at higher strain [16]. The sense of inclination of the shear bands was dependent on the particular $\{1\,1\,1\}\langle 1\,1\,2\rangle$ orientation in which they developed (Fig. 9). The texture inside the shear bands consisted of the Goss orientation and the two symmetrical $\{1\,1\,1\}\langle 1\,1\,2\rangle$ components with varying intensities, but no additional orientations appeared [16]. These two observations, i.e. the correlation of shear band inclination with crystal orientation and the occurrence of only a limited number of crystal orientations inside the shear bands, revealed the crystallographic nature of the observed shear bands. Therefore, it can be assumed that the shear bands are so-called copper-type shear bands that develop due to geometrical softening as described by Dillamore et al. [17].

3.3. Evolution of the Goss orientation during cold rolling

In the 89% de formed samples, two types of Goss-oriented regions were discovered. Most of the Goss grains were situated inside the shear bands that developed in late stages of the rolling process (Fig. 10). The low EBSD pattern quality indicated that the stored strain energy of these Goss grains is high. Another type of Goss grains was found between microbands (Fig. 11), i.e. in regions with a high EBSD pattern quality indicating a low stored strain energy. In most cases, these Goss grains were found embedded in one of the two symmetrical $\{1\,1\,1\}\langle 1\,1\,2\rangle$ orientations. After the highest deformation degree of 89%, most of the remaining Goss-oriented crystal volume was surrounded by high-angle grain boundaries. The average diameter of the Goss residuals was about 0.3 µm.

In the less deformed material without shear bands the evolution of the initially Goss-oriented volume was clearly related to the development of microbands (Figs. 6,7 and 12). At some places the Goss-oriented regions were already completely surrounded by high-angle grain boundaries (Fig. 13). Other Goss-oriented regions partly showed

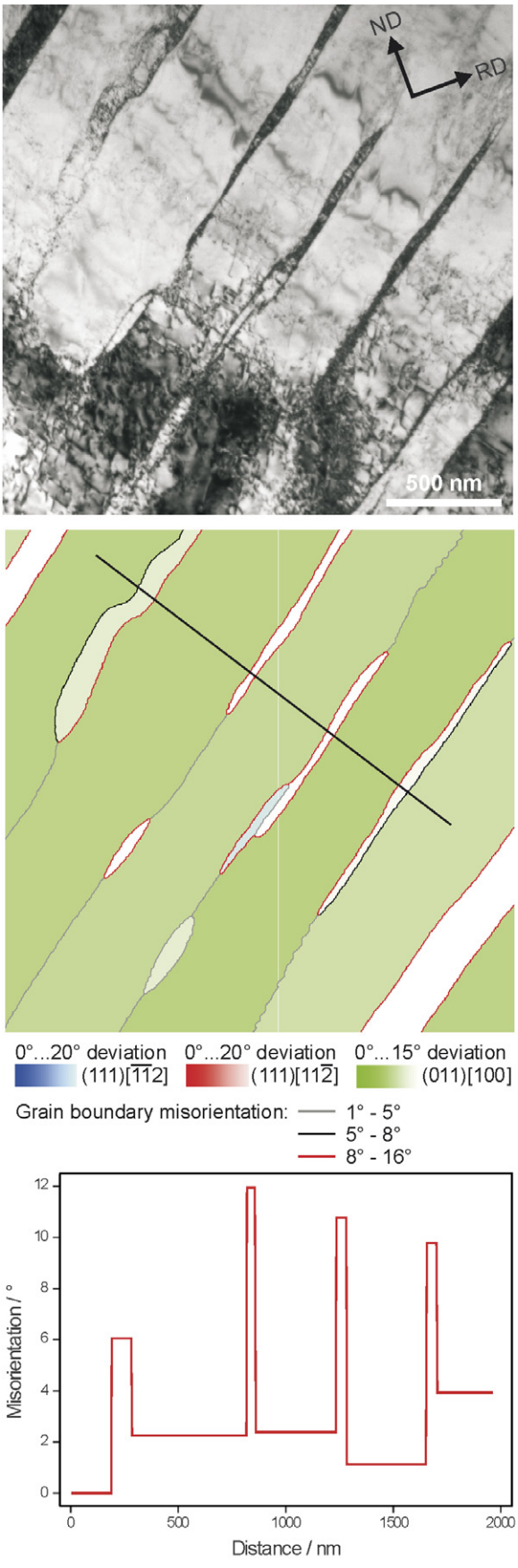

Fig. 7. Microbands with open and closed parts in a 55% deformed initially Goss-oriented FeSi single crystal. (a) TEM bright field image. (b) Crystal orientation map. (c) Misorientation profile along the line in (b).

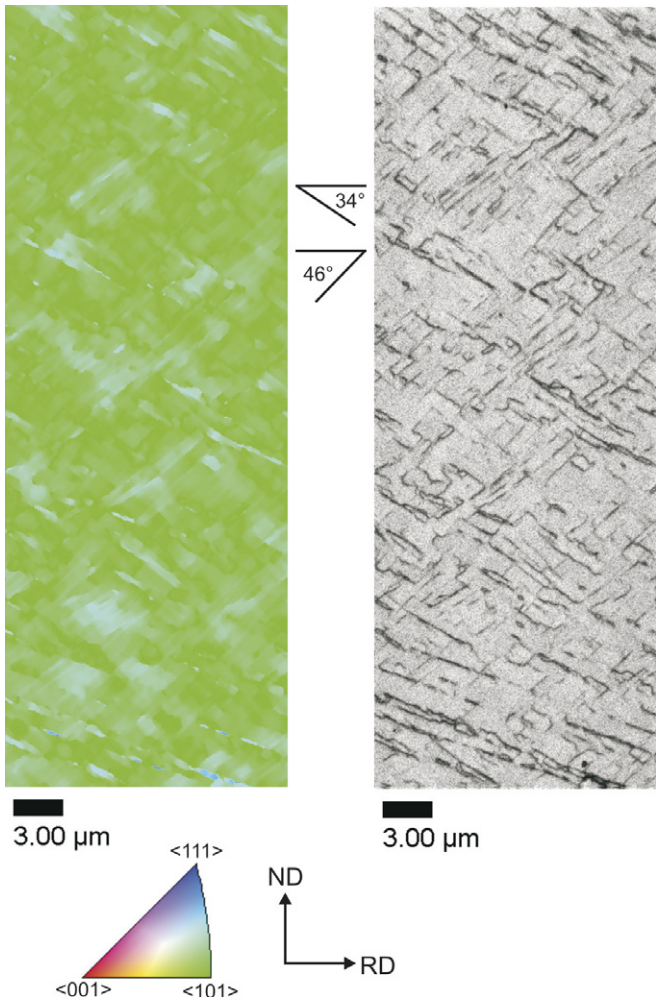

Fig. 8. 55% deformed, initially Goss-oriented FeSi single material with a region characterised by two crossing sets of linear microstructural features that are supposed to be early stages of microband evolution. (a) Inverse pole figure map for the normal sample direction as obtained by EBSD. (b) EBSD pattern quality map showing microbands as linear features with low EBSD pattern qualities.

high-angle grain boundaries and were partly in a continuous orientation gradient (Fig. 13). This indicated that the Goss grains between the microbands first form high-angle grain boundaries across the microbands, while parallel to the microbands the orientation continuously changed. Across the high-angle grain boundaries the orientation difference frequently approached 35°, which is the misorientation between the Goss and the two $\{1\,1\,1\}\langle 1\,1\,2\rangle$ orientations. TEM investigations showed that the high-angle grain boundaries of the Goss grains are very sharp (Fig. 14).

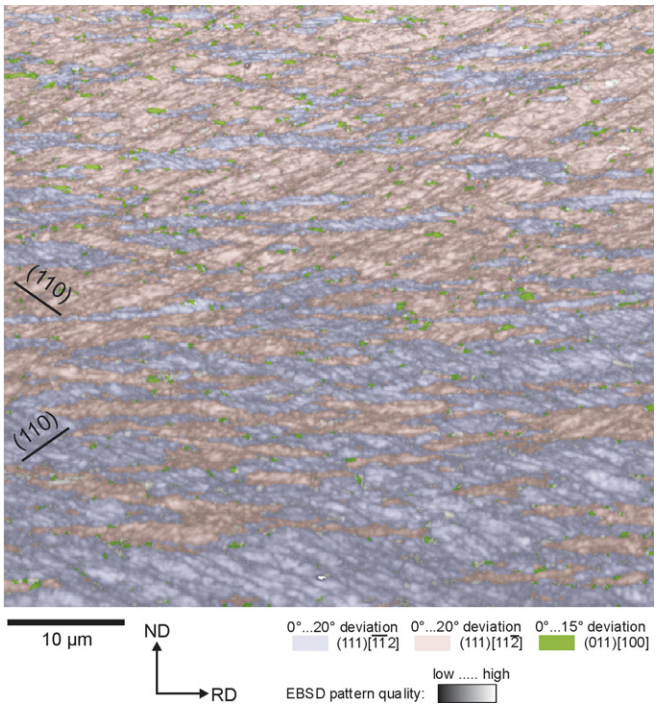

Fig. 9. Correlation of the inclination direction of shear bands with the particular $\{111\}\langle 112\rangle$ orientation in the 89% deformed material. The orientations of the $\{110\}$ planes are indicated (see also Fig. 16). EBSD pattern quality map combined with the corresponding crystal orientation. Shear bands are visible as linear features with a low EBSD pattern quality.

4. Discussion

4.1. Stability of the Goss orientation during cold rolling

Taylor-type as well as corresponding crystal-plasticity finite element simulations showed that bcc crystals with Goss orientation are unstable under plane strain deformation [12,13]. More precisely, while the mathematically *exact* $\{110\}\langle 001\rangle$ orientation is stable under ideal plane strain loading, very small deviations from the exact Goss orientation or slight changes in the boundary conditions, e.g. friction, lead to a transverse rotation towards the two symmetrical $\{111\}\langle 112\rangle$ orientations [18,12]. In contrast, under pure shear strain deformation, the $\{111\}\langle 112\rangle$ orientations rotate into the Goss orientation, which is stable in this case [12,18]. In general, cold rolling can be approximated as a plane strain deformation state, if shear strain due to friction at the sheet surface is negligible. Therefore, in this study, the initial Goss orientation should be unstable during cold rolling. Indeed, this was observed for the major volume fraction of the cold rolled silicon steel sheet (Figs. 3 and 9–11). However, about 2.0–2.5% of the material formed small islands with Goss orientation (considering a misorientation up to 15°) even after as much as 89% thickness reduction of an initially Goss-oriented single crystal (Figs. 9–11).

In the following sections the origin of the remaining Goss-oriented crystal volumes is discussed with respect to two conceivable mechanisms corresponding to the two types of observed Goss regions. First, the generation of the Goss orientation in shear bands is presented. Second, we discuss the retention of small Goss-oriented crystal volumes between microbands.

4.2. Formation of Goss grains inside of shear bands

The role of shear bands in the context of the Goss texture formation in silicon steel has already been investigated by Haratani et al. [19] and Ushioda and Hutchinson [20]. However, they could not resolve the microstructure of the shear bands in the cold rolled state. In this study, it

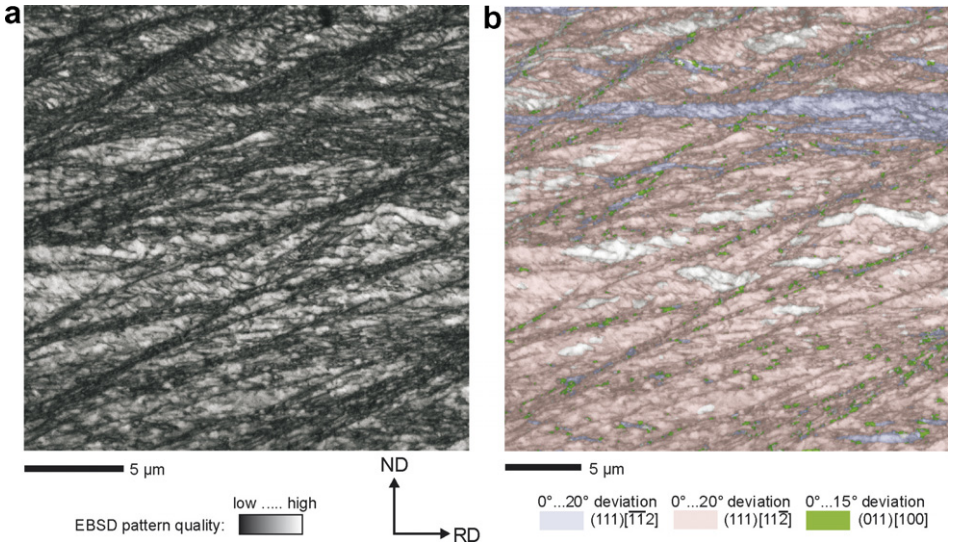

Fig. 10. Goss grains inside of shear bands in the 89% deformed material. (a) EBSD pattern quality map showing shear bands as regions with low EBSD pattern qualities. (b) Same map as in (a) combined with the corresponding crystal orientation. The Goss-oriented regions are aligned along the shear bands.

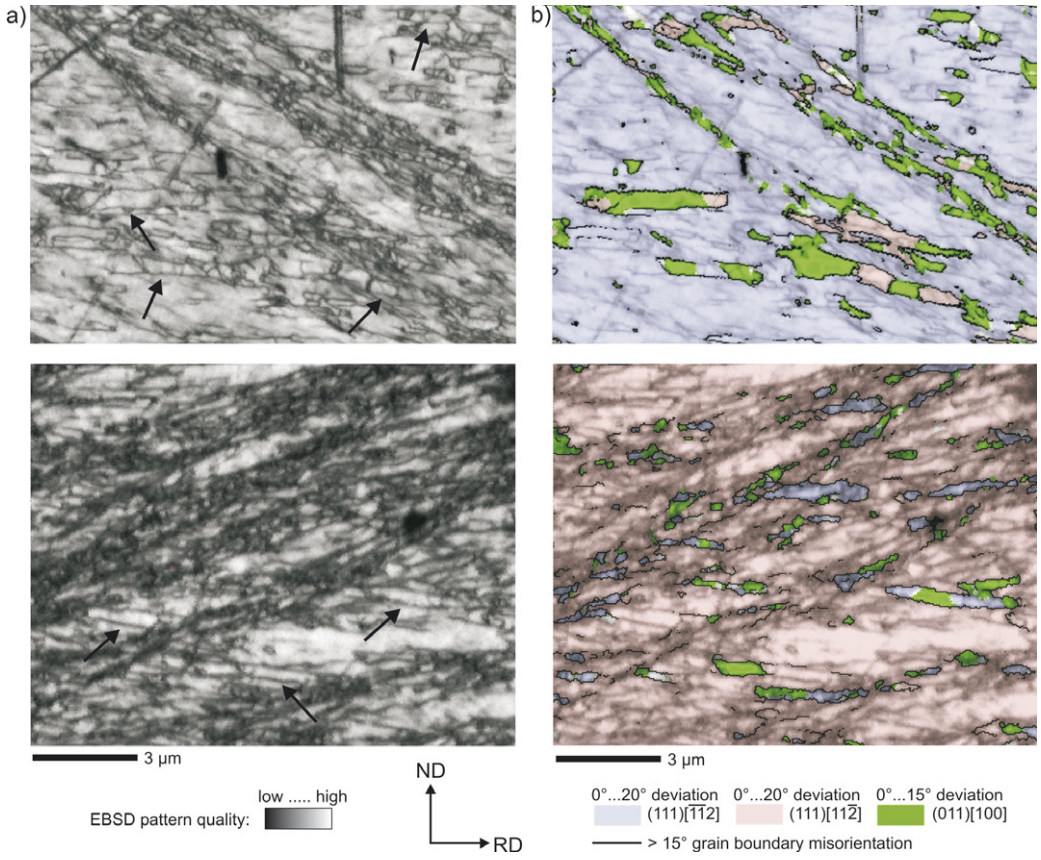

Fig. 11. Goss grains between microbands in the 89% deformed material. (a) EBSD pattern quality map showing parallel microbands as parallel linear features with low pattern quality (see arrows). In addition, shear bands are present. (b) Same map as in (a) combined with the corresponding crystal orientation. Goss grains that are aligned inside of shear bands are also visible.

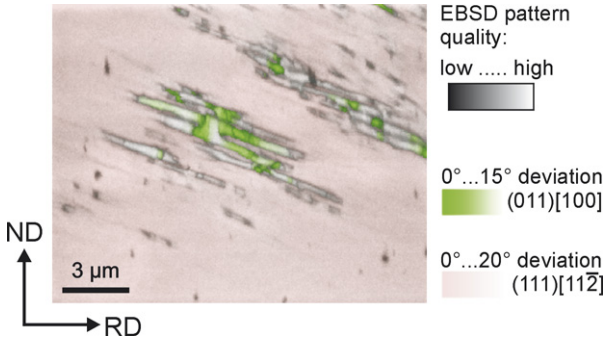

Fig. 12. Relation of microbands and Goss-oriented crystal volumes. 55% deformed material. EBSD pattern quality map combined with the corresponding crystal orientation.

was observed that a part of the Goss grains that were found after high strain was aligned inside shear bands. This observation, and the fact that shear bands started to form only after a strain of about 77% thickness reduction, indicated that the Goss orientation formed due to the local shear deformation in the shear bands. Therefore, it was assumed that, at first, the initial Goss orientation rotates to the two $\{1\,1\,1\}\langle 1\,1\,2\rangle$ orientations. At higher deformation degrees, when the shear bands are formed, the $\{1\,1\,1\}\langle 1\,1\,2\rangle$ orientations then rotate back to the Goss orientation due to the local shear strain in the shear bands. In this context, the question arose why only part of the material within the shear bands rotated back to the Goss orientation while the rest remained in the $\{1\,1\,1\}\langle 1\,1\,2\rangle$ orientations [16]. The alternative possibility that the initial Goss orientation was retained within the shear bands could be excluded because shear bands first formed at a strain when most of the Goss orientation had already rotated into the $\{1\,1\,1\}\langle 1\,1\,2\rangle$ orientations.

4.3. Development of microbands and retention of the Goss orientation between microbands

Goss grains, which are surrounded by high-angle grain boundaries, were found between microbands in the highest deformed material (Figs. 11 and 14). In earlier deformation stages, Goss-oriented regions were also observed between microbands (Figs. 6, 7, 12 and 13). These observations indicated that the retention of the initial Goss orientation and the development of microbands are closely related. In the following it is outlined how the microbands develop, and a tentative explanation is given that describes how the Goss orientation might be retained between the microbands.

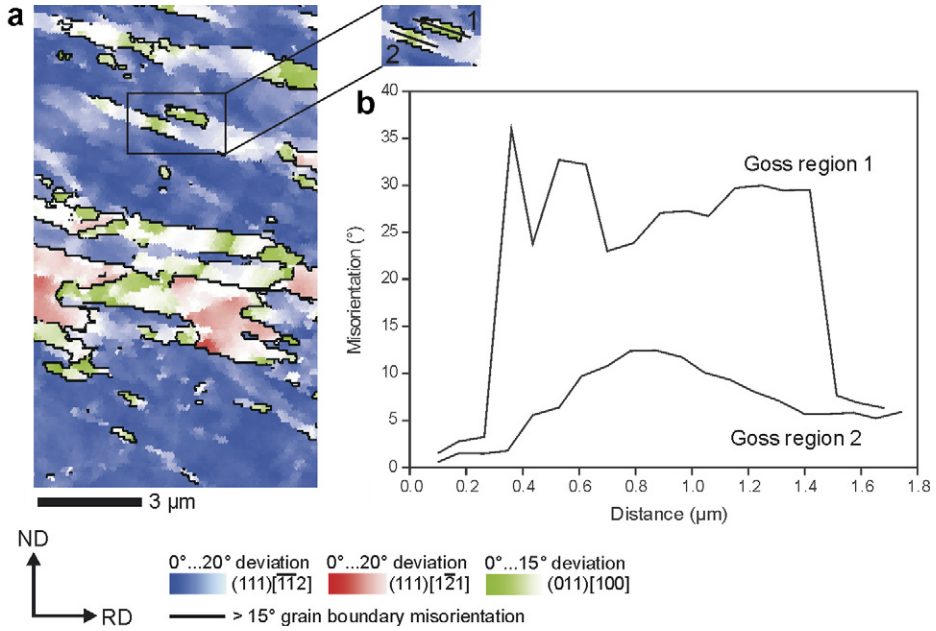

Fig. 13. (a) Goss-oriented regions in the 70% deformed material. (b) Misorientation profiles for Goss region 1, which is completely surrounded by high-angle grain boundaries, and for Goss region 2, which forms an orientation gradient with the $\{1\,1\,1\}\langle 1\,1\,2\rangle$ matrix.

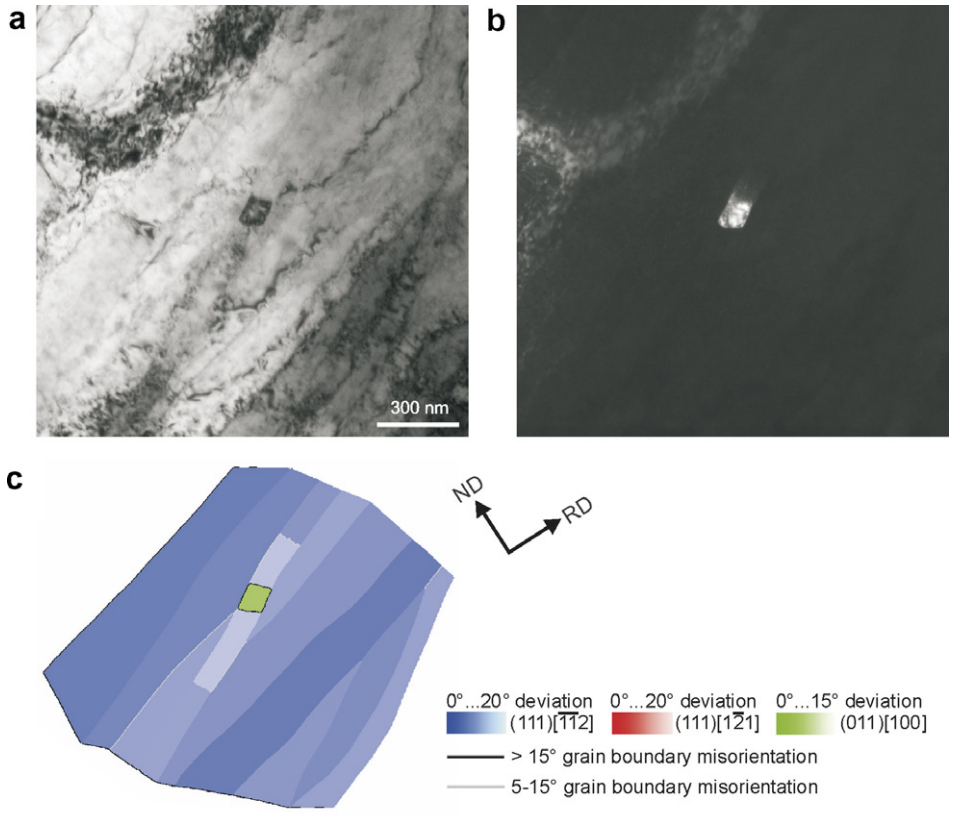

Fig. 14. Goss grain surrounded by sharp high-angle grain boundaries in the 66% deformed material. (a) TEM bright field image. (b) TEM dark field image. (c) Crystal orientation map for the same area as in (a) and (b). High-angle grain boundaries are marked in black, low-angle grain boundaries in grey.

In a first step, a fully constrained Taylor model was used in order to estimate which slip systems are active during the transverse lattice rotation from the $\{1\,1\,0\}\langle 0\,0\,1\rangle$ towards the two $\{1\,1\,1\}\langle 1\,1\,2\rangle$ crystal orientations. The 12 $\{1\,1\,0\}\langle 1\,1\,1\rangle$ and the 12 $\{1\,1\,2\}\langle 1\,1\,1\rangle$ slip systems were taken into account for the determination of the Taylor factor, the

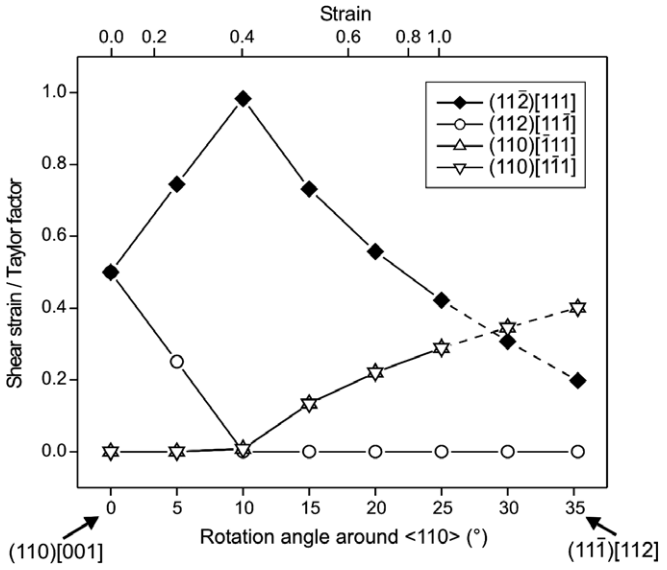

Fig. 15. Shear strain on different slip systems normalized by the Taylor factor as a function of rotation from (1 1 0)[0 0 1] to (1 1 $\bar{1}$)[1 1 2] around the ⟨1 1 0⟩ crystal direction. Strains corresponding to the lattice rotation are indicated at the upper axis. A fully constraint Taylor model with 24 slip systems for a bcc crystal was used to calculate the active slip systems.

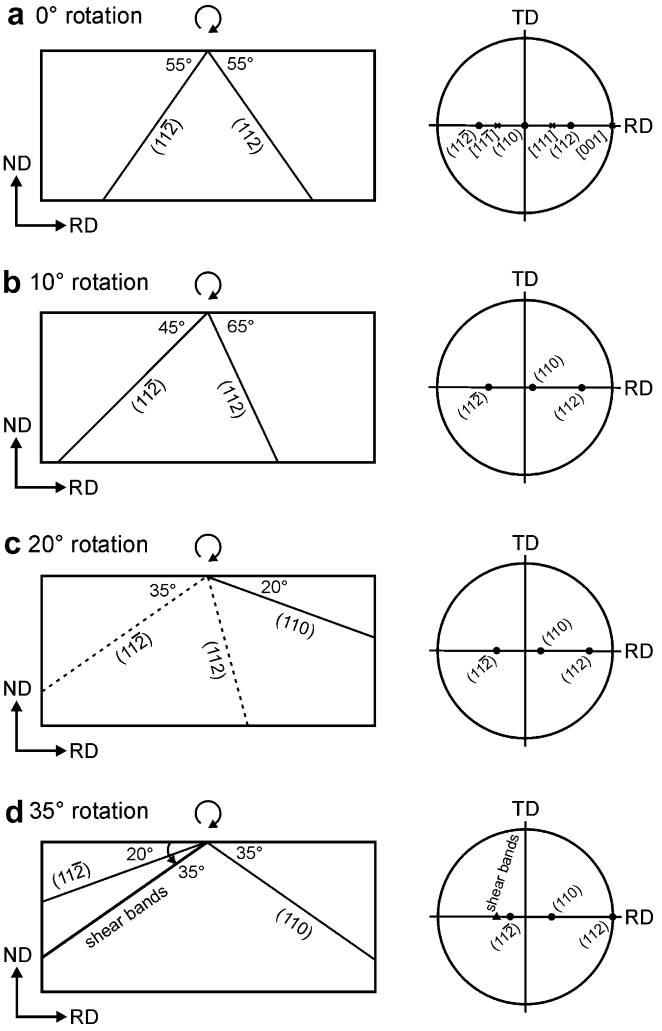

Fig. 16. Activity of glide planes and shear bands for four different rotation angles from (1 1 0)[0 0 1] to (1 1 $\bar{1}$)[1 1 2] around the ⟨1 1 0⟩ crystal direction.

active slip systems and the corresponding shear strain for each slip system. The main finding of the Taylor-type calculations was that the gradual orientation change from the Goss orientation to a {1 1 1}⟨1 1 2⟩ crystal orientation is characterised by, first, a concentration of the dislocation activity on only one particular glide system for small rotation angles, and second, by a discontinuous transition of the second and third active slip systems with further increase of rotation and accordingly deformation (Fig. 15). Note that the fully constrained Taylor model gives the {11 11 8}⟨4 4 11⟩ orientation as the stable end orientation for the Goss orientation. Therefore, in Fig. 15 the strains that correspond to the lattice rotation were only given for a rotation of up to 25°. In contrast to the simulations, the experimental results showed that for larger strains the lattice rotation continues towards the {1 1 1}⟨1 1 2⟩ orientations (Fig. 3).

The microstructure observations, combined with the results obtained from the Taylor-type calculation on the active slip systems, yielded the following ideas on the activity of glide planes and shear bands and on microband development during the rolling process (Figs. 15 and 16). In the initial Goss orientation, slip starts on the two {1 1 2} planes that are inclined by 55° to the rolling direction (Figs. 15 and 16a). In Fig. 8 crossing linear structures (resp. early microbands) possibly reflect this initial activity on two {1 1 2} planes after some rotation had already occurred since the observed inclination is smaller than the theoretical 55°. During further rotation, the activity on one of these glide planes ceases, while activity on the other glide plane that rotates toward smaller inclination angles increases (Figs. 15 and 16b). The continuing activity on, in this example, (1 1 $\bar{2}$)[1 1 1] (Figs. 15 and 16a–c) causes the formation of parallel microbands (Figs. 5 and 6). The significance of {1 1 2} glide planes for the formation of microbands is confirmed by the observation that the microband habit plane is close to {1 1 2}, with a small deviation possibly due to some amount of pencil glide. According to Chen et al. [15], one set of microbands forms when the habit plane of the observed microband has the largest Schmid factor and when one ⟨1 1 1⟩ slip direction is intensively activated in this plane. This is valid for a Goss-oriented single crystal. For more than 10° of rotation, the activity on (1 1 $\bar{2}$) decreases, while that on the (1 1 0) glide plane increases (Figs. 15 and 16c). After the full 35° rotation from Goss to {1 1 1}⟨1 1 2⟩, the main slip activity is now on the (1 1 0) plane and therefore microband formation is assumed to have terminated. At this stage, shear bands form symmetrically to the (1 1 0) plane that is inclined by 35° to the rolling direction (Fig. 16d). This scenario is accordingly valid for the rotation of the Goss orientation to the other {1 1 1}⟨1 1 2⟩ crystal orientation.

Dillamore et al. [21] explained the retention of the initial crystal orientation by a transition band model. Their idea is that an unstable starting orientation rotates toward symmetrical orientations in two directions and the initial orientation is retained in a transition band between the stable end orientations. In the present study, this would correspond to a situation where the initial Goss orientation persists in a transition band between the two symmetrical $\{1\,1\,1\}\langle 1\,1\,2\rangle$ orientations. However, we found that the Goss regions that were retained between microbands were mostly situated in one $\{1\,1\,1\}\langle 1\,1\,2\rangle$ orientation, not between the two different $\{1\,1\,1\}\langle 1\,1\,2\rangle$ components. Thus, the Dillamore transition band model does not explain the observed retention of the Goss orientation between microbands. Therefore, we suggest the following tentative explanation for the Goss retention, which is based on the idea that in a small crystal volume a different set of slip systems is active compared with in the surrounding material. While experimentally the Goss orientation is unstable under plane strain loading conditions, the mathematically exact Goss orientation under exact plane strain loading conditions does not rotate, because the opposite rotations towards the two symmetrical $\{1\,1\,1\}\langle 1\,1\,2\rangle$ orientations exactly compensate. However, even a slight deviation from exact Goss or a slight deviation from the exact plane strain condition, e.g. due to local stress heterogeneities, favours one of the sets of slip systems and causes a rotation of the Goss orientation towards one of the stable end positions. On the macroscopic scale, depending on the macroscopic stress conditions, parts of the originally Goss-oriented crystal rotate in one direction while other parts rotate in the other direction towards $\{1\,1\,1\}\langle 1\,1\,2\rangle$. Locally, however, stress heterogeneities, e.g. due to microbands that act as dislocation obstacles, might activate that set of slip systems that causes lattice rotation into the opposite direction. This leads to the situation displayed in Fig. 17: a small crystal volume, in which different slip systems are active compared with in the surrounding material, might be temporarily considered as a rigid inclusion (Fig. 17a). The surrounding matrix rotates in one direction, thereby imposing a similar rotation on the inclusion in the form of a rigid body rotation (Fig. 17b). Inside this so-called inclusion, a different, but symmetrical set of slip systems causes the exact opposite lattice rotation, thus balancing out the externally imposed rotation (Fig. 17c). This leads to a zero net rotation, and thus the initial Goss orientation is retained in that small crystal volume. This process is, however, quite critical as the internal rotation in the small regions must always be slightly ahead of the macroscopic external rotation. Otherwise the set of slip systems that causes lattice rotation in the same sense as the matrix would be activated and the Goss orientation would no longer be stable, but would rotate in the same direction as the matrix. In fact, the experimental data for low rolling degrees show that there are more Goss-oriented regions between microbands in the less strained material (Fig. 6). In some places the retained Goss areas are embedded in a matrix of one of the $\{1\,1\,1\}\langle 1\,1\,2\rangle$ components, but small areas of the other $\{1\,1\,1\}\langle 1\,1\,2\rangle$ components can be found on both ends. This observation supports the idea of a different set of slip systems being active in small areas between microbands, causing correspondingly different lattice rotations. The reason for different deformation characteristics in small, confined areas might be local stress heterogeneities. However, more work is required to understand the details of this process.

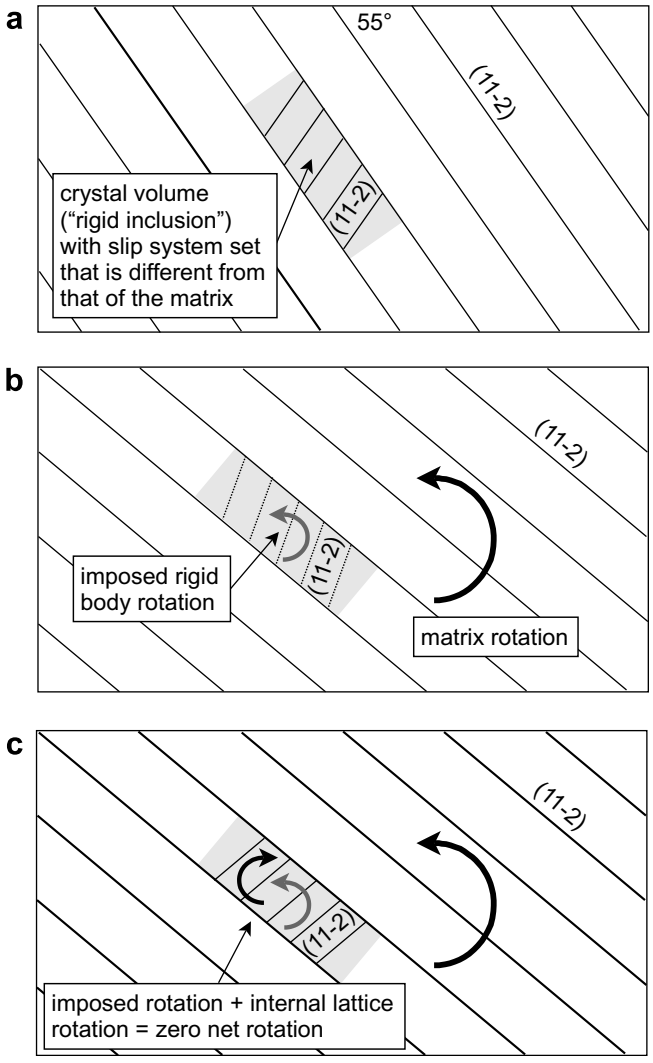

Fig. 17. Tentative idea for the retention of Goss-oriented crystal volumes between microbands. The mechanism is based on the idea that in a small crystal volume an internal lattice rotation and an externally imposed rigid body rotation compensate each other, resulting in zero net rotation. For a detailed description see the text.

Concluding, we suppose that the origin of Goss-oriented regions between microbands is the initial Goss orientation of the single crystal that is retained in small crystal volumes. This is in contrast to the origin of the Goss-oriented regions inside shear bands that rotate back to the Goss orientation after a change in the deformation mode from plain strain to shear.

5. Summary and conclusions

An initially Goss-oriented FeSi single crystal was cold rolled to a thickness reduction of 89%. In the course of rolling, most of the material rotated into the two symmetrically equivalent $\{1\,1\,1\}\langle 1\,1\,2\rangle$ orientations. However, a weak Goss texture component was observed in the highly deformed material, even though the Goss orientation is not stable under plane strain deformation. Investigation of the deformed microstructure led to the identification of two types of Goss-oriented regions with different origins. One type was found in highly strained material inside shear bands. These Goss regions formed in the shear bands that developed at thickness reductions of more than 70%. The second type of Goss regions was situated between microbands, i.e. in regions with low stored strain energy. The origin of the Goss orientation between the microbands is the initial Goss orientation. A tentative explanation outlines how these Goss-oriented regions were retained from the initial Goss orientation of the single crystal. It is proposed that in small areas between microbands a different set of slip systems is active compared with in the surrounding material. Under favourable conditions the rotation in this area compensates the opposite rigid body rotation imposed by the surrounding material and the initial Goss orientation is retained.

The sharp Goss orientation that develops during secondary recrystallisation in industrially processed silicon steel has its origin in the hot rolling stage. In this study, two types of Goss regions were observed after cold rolling of an initially Goss-oriented single crystal. Provided that the results on single crystals can be transferred to polycrystalline material, it might be concluded that the Goss-oriented regions that are found between microbands and that are assumed to be stable during cold rolling have special significance for the formation of Goss grains in the primary recrystallised material, and, consequently, for the abnormal growth of Goss grains during secondary recrystallisation. If the newly formed Goss grains inside the shear bands were specifically relevant, then the removal of the surface layer would not change the formation of Goss grains during primary recrystallisation [5,1,6].

Acknowledgement

The authors gratefully acknowledge financial support by ThyssenKrupp Electrical Steel GmbH. The same company also kindly provided the sample material for this research project.

References

[1] Mishra S, Därmann C, Lücke K. Acta Metall 1984;32:2185.
[2] Matsuo M, Sakai T, Yozo S. Metall Trans 1986;17A:1313.
[3] Shimizu Y, Ito Y, Iida Y. Metall Trans 1986;17A:1323.
[4] Matsuo M. ISIJ Int 1989;29:809.
[5] Böttcher A, Lücke K. Acta Metall Mater 1993;41:2503.
[6] Pease NC, Jones DW, Wise MHL, Hutchinson WB. Met Sci 1981;15:203.
[7] Dorner D, Zaefferer S, Lahn L, Raabe D. J Magn Magn Mater 2006;304:183.
[8] May JE, Turnbull D. Trans Metall Soc AIME 1958;212:769.
[9] Seidel L, Hölscher M, Lücke K. Texture Microstruct 1989;11:171.
[10] Zaefferer S, Chen N. Solid State Phenom 2005;105:29.
[11] Dunn CG. Acta Metall 1954;2:173.
[12] Raabe D, Zhao Z, Park S-J, Roters F. Acta Mater 2002;50:421.
[13] Hölscher M, Raabe D, Lücke K. Steel Res 1991;62:567.
[14] Zaefferer S. J Appl Cryst 2000;33:10.
[15] Chen QZ, Ngan AHW, Duggan BJ. Proc R Soc London A 2003;459:1661.
[16] Dorner D, Zaefferer S. Solid State Phenom 2005;105:239.
[17] Dillamore IL, Roberts JG, Bush AC. Met Sci 1979;13:73.
[18] Hölscher M, Raabe D, Lücke K. Acta Metall Mater 1994;42:879.
[19] Haratani T, Hutchinson WB, Dillamore IL, Bate P. Met Sci 1984;18:57.
[20] Ushioda K, Hutchinson WB. ISIJ Int 1989;29:862.
[21] Dillamore IL, Morris PL, Smith CJE, Hutchinson WB. Proc R Soc London A 1972;329:405.

Available online at www.sciencedirect.com
SCIENCE DIRECT
Journal of Magnetism and Magnetic Materials 304 (2006) 183–186
Journal of magnetism and magnetic materials
www.elsevier.com/locate/jmmm

Overview of Microstructure and Microtexture Development in Grain-oriented Silicon Steel

Dorothée Dorner[a], Stefan Zaefferer[a,*], Ludger Lahn[b], Dierk Raabe[a]

[a]*Max-Planck-Institut für Eisenforschung, Max-Planck-Strasse 1, 40237 Düsseldorf, Germany*
[b]*ThyssenKrupp Electrical Steel GmbH, Kurt-Schumacher-Strasse 95, 45881 Gelsenkirchen, Germany*

Available online 13 March 2006

Abstract

This paper outlines the development of the microstructure and microtexture of grain-oriented silicon steel during the industrial production process. In particular the evolution of the Goss orientation was studied in industrial material as well as in single crystal experiments.

PACS: 61.14.−x; 75.50.Bb; 81.40.Ef; 92.10.Ns

Keywords: Grain-oriented silicon steel; Goss orientation; EBSD

1. Introduction

The grain-oriented silicon steel is a soft magnetic material that is used as the core material in electrical transformers. It is characterized by a pronounced Goss texture, i.e. a $\{110\}\langle 0\,0\,1\rangle$ preferred crystal orientation. This sharp texture develops due to a discontinuous or abnormal Goss grain growth during a high-temperature annealing at the end of the industrial production process. Although it is a matter of intensive basic and applied research since more than 50 years, there is no general agreement on the origin of preferred growth of the Goss grains. It is known, however, that the inheritance of Goss orientation from early production stages plays an important role, as it was shown by Böttcher and Lücke in Ref. [1] who removed the Goss-containing surface layer of the hot rolled material with the result that abnormal Goss grain growth did not take place after further processing. Therefore, in this contribution we intend to outline the evolution of the Goss orientation in industrially processed grain-oriented silicon steel along the various production stages, i.e. hot rolling, cold rolling, primary annealing, and secondary annealing. Furthermore, experiments are described in which the evolution of a Goss-oriented single crystal was tracked during the cold rolling and primary annealing in order to gain more information on the origin of abnormal Goss grain growth. All observations the of microstructure and microtexture were carried out by means of a high resolution and high speed EBSD (electron backscatter diffraction) analysis system (TSL OIM software; JEOL 6500F field emission gun scanning electron microscope) that allows to map very large areas, in order to detect the very rare Goss grains, as well as to precisely reconstruct the microstructure of heavily deformed samples.

2. Microstructure and microtexture evolution

2.1. Hot rolling

Industrial material: During hot rolling the Goss orientation originates due to shear deformation close to the strip surface [1–5]. Our microtexture measurements revealed some quite large Goss grains without visible substructure (Fig. 1). However, other Goss grains are much smaller, reveal a substructure or an orientation gradient.

Single crystal experiments: The idea of our single crystal experiments is visualized in Fig. 2: we grabbed one of the Goss grains in the hot rolled material and deformed and

*Corresponding author. Tel.: +49 211 6792 803.
E-mail address: zaefferer@mpie.de (S. Zaefferer).

0304-8853/$ - see front matter © 2006 Elsevier B.V. All rights reserved.
doi:10.1016/j.jmmm.2006.02.116

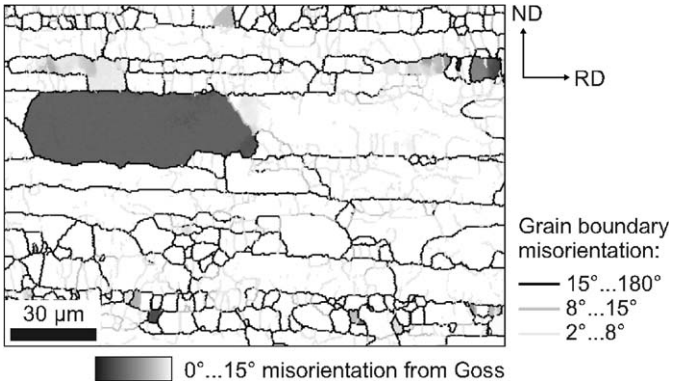

Fig. 1. Large Goss grain in industrially hot rolled silicon steel. Crystal orientation map including grain boundaries. RD: rolling direction; ND: normal direction.

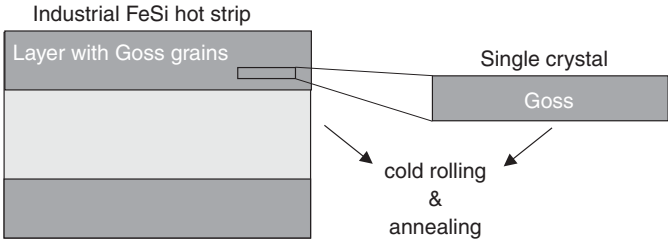

Fig. 2. Idea of single crystal experiments.

annealed it in the same way as it was done with the industrial polycrystalline silicon steel. Experimentally this was done by growing a macroscopic Goss-oriented single crystal ($20 \times 50 \times 2.2\,mm^3$) which was then used for cold rolling [6,7] and annealing experiments.

2.2. Cold rolling

Industrial material: As already known from earlier studies on industrially cold rolled silicon steel, the major texture components after cold rolling are the α-fibre and the γ-fibre [1,8,9,4]. However, our microtexture measurements revealed that small Goss-oriented areas are also present in the cold rolled microstructure. The area fraction of the Goss orientation is about 1% taking into account a maximum misorientation from exact Goss of 15°. This weak Goss component was not detected in earlier studies due to the lower resolution of the X-ray diffraction compared to the EBSD technique. Furthermore, we observed that the occurrence of Goss-oriented areas was restricted to regions with orientations close to $\{111\}\langle 1\,1\,2\rangle$ (Fig. 3). Most of the Goss grains were aligned along shear bands, however, very few Goss grains appeared to occur in less strained areas outside of shear bands.

Single crystal experiments: Cold rolling of a Goss-oriented single crystal resulted in a crystal rotation into the two symmetrically equivalent $\{111\}\langle 1\,1\,2\rangle$ texture components as already reported by Dunn [10]. But we found that Goss-oriented areas were still present in the

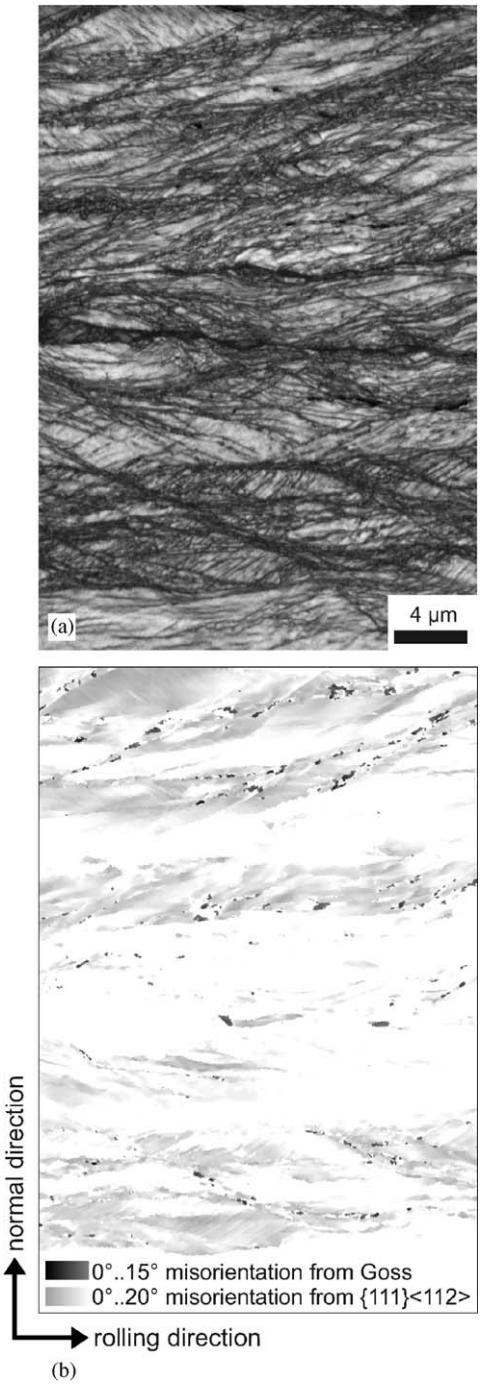

Fig. 3. Industrial silicon steel: (a) Microstructure with characteristic shear bands. EBSD pattern quality map: darker areas represent a higher dislocation density; (b) Crystal orientation map. The Goss-oriented areas occur only next to $\{111\}\langle 1\,1\,2\rangle$-oriented areas.

highly strained material with a fraction of 2.2–2.6%, although the Goss orientation is not stable under plane strain deformation [9,11]. In particular, we observed two types of Goss grains (Fig.4). Goss grains inside of shear bands newly formed during deformation at high strain. Whereas we supposed that those Goss grains that were found between microbands were retained during cold rolling [6,7].

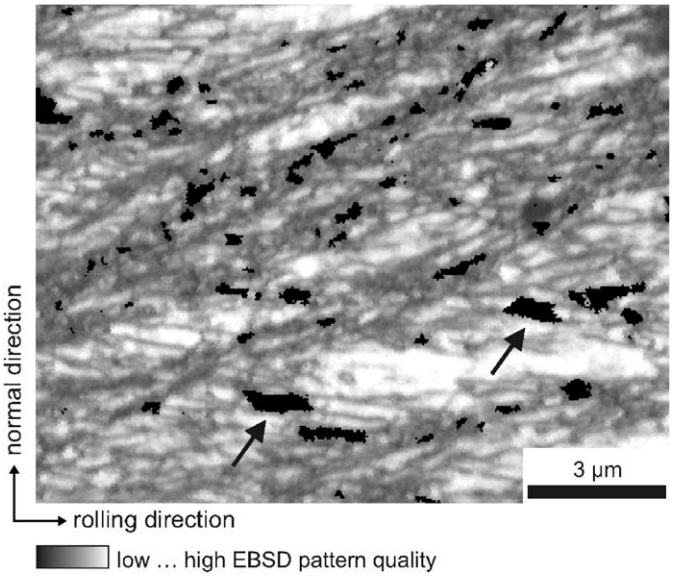

Fig. 4. Single crystal experiments. Goss-oriented areas in a 89% deformed, originally Goss-oriented single crystal. The Goss grains are situated both inside of shear bands and between microbands (arrows). EBSD pattern quality map; Goss-oriented areas are marked in black.

2.3. Primary annealing

Industrial material: After primary recrystallization the Goss orientation forms a minor texture component in high permeability grade material and is a one of the main texture components in conventional grade silicon steel. In both grades, the major texture component is the γ-fibre e.g. Ref. [3]. Microtexture analysis showed that the Goss grains are not larger than other grains, i.e. they do not have a size advantage during secondary annealing [12].

Single crystal experiments: In contrast to the industrially processed material, in the deformed and annealed originally Goss-oriented single crystal, the Goss orientation is the strongest texture component. Our microstructure analysis revealed that the Goss grains between the microbands are likely to form nuclei for primary recrystallization. The Goss grains inside of shear bands mostly disappeared.

2.4. Secondary annealing

Industrial material: During the final high temperature annealing, normal grain growth is inhibited by particle pinning of grain boundaries e.g. Ref. [3]. However, some of the Goss grains that are present in the primary recrystallized material can unpin and grow abnormally giving rise to the formation of a sharp and strong Goss texture.

3. Origin of abnormal Goss grain growth

Abnormal Goss grain growth can be due to a growth selection or an oriented nucleation mechanism. Most existing models of abnormal Goss grain growth propose a growth selection mechanism based on special grain boundary properties, that are e.g. the $\Sigma 9$ grain boundary theory [13,14] or the high angle grain boundary theory [15]. However, these theories cannot explain all experimental observations on abnormal Goss grain growth as it was recently outlined by Zaefferer and Chen [16]. Thus, we assume that there is another, probably an oriented nucleation mechanism leading to abnormal Goss grain growth. We suspect that the Goss grains are characterized by a special microstructure, e.g. dislocation structure, which originates in the early production stages and is inherited through the production process. Our search for special microstructural properties of Goss grains is facilitated by the use of single crystals as the starting material, because in this case the number of Goss grains is higher in the cold rolled and in the primary recrystallized states.

4. Discussion

Our EBSD investigations rendered possibly a detailed analysis of the microstructure and microtexture of particularly the deformed state of silicon steel. We found that in the cold rolled industrial material Goss-oriented areas only occurred in the neighborhood of $\{111\}\langle 1\,1\,2\rangle$ grains. This observation implied that findings from our single crystal experiments, where the texture components were only Goss and $\{111\}\langle 1\,1\,2\rangle$, can possibly be transferred to polycrystalline material. In the industrial material, most of the Goss grains were aligned along shear bands, but some appeared not to be related to shear bands. This was consistent with our observation on the originally Goss-oriented single crystal material. In this case after deformation two types of Goss grains were found: in shear bands and between microbands. The Goss grains in shear bands newly developed during deformation. Whereas those between microbands were retained during cold rolling. Their primary recrystallization behaviour was also different. The Goss grains between microbands formed the recrystallisation nuclei, whereas the Goss grains in the shear bands mostly disappeared during annealing. This observation is in contrast to that of Ref. [8] who stated the formation of new Goss-oriented crystals in shear bands. This indicates that possibly some ideas about the formation of Goss grains have to be revised.

5. Summary

In this study the evolution of the microstructure and microtexture of silicon steel was investigated using EBSD. In particular the development of the Goss orientation was tracked in both industrial material and single crystal material. A study on the evolution of the Goss orientation throughout all production stages is important with regard to the question of the origin of abnormal Goss grain growth, because the Goss orientation originates during hot rolling and is inherited to the final secondary annealing. For the industrial material, we found that the occurrence and the amount of the Goss orientation is related to the

{111}⟨1 1 2⟩ orientation. The most important finding for the single crystal was that two types of Goss grains occurred in the cold rolled state, which also showed different primary recrystallization behaviour. We supposed that results obtained from single crystal experiments can be transferred to industrial material and that they offer the potential to investigate the microstructure of individual Goss grains helping to solve the question of the origin of abnormal Goss grain growth.

Acknowledgment

Financial support by ThyssenKrupp Electrical Steel GmbH is gratefully acknowledged.

References

[1] A. Böttcher, K. Lücke, Acta Metall. Mater. 41 (1993) 2503.
[2] M. Matsuo, T. Sakai, S. Yozo, Metall. Trans. 17A (1986) 1313.
[3] M. Matsuo, ISIJ Int. 29 (1989) 809.
[4] S. Mishra, C. Därmann, K. Lücke, Metall. Trans. 17A (1986) 1301.
[5] Y. Shimizu, Y. Ito, Y. Iida, Metall. Trans. 17A (1986) 1323.
[6] D. Dorner, L. Lahn, S. Zaefferer, Textures of Materials—ICOTOM, vol. 14, pp. 1061, Trans Tech Publ. 2005.
[7] D. Dorner, S. Zaefferer, D. Raabe, Acta Mater., in revision.
[8] T. Haratani, W.B. Hutchinson, I.L. Dillamore, P. Bate, Metal Sci. 18 (1984) 57.
[9] M. Hölscher, D. Raabe, K. Lücke, Steel Res. 62 (1991) 567.
[10] C.G. Dunn, Acta Metall. 2 (1954) 173.
[11] D. Raabe, Z. Zhao, S.-J. Park, F. Roters, Acta Mater. 50 (2002) 421.
[12] N. Chen, S. Zaefferer, L. Lahn, K. Günther, D. Raabe, Acta Mater. 51 (2003) 1755.
[13] H. Homma, B. Hutchinson, Acta Mater. 51 (2003) 3795.
[14] T. Nakayama, Y. Ushigami, Mater. Sci. Forum 47 (1992) 413, 94.
[15] Y. Hayakawa, J.A. Szpunar, Acta Mater. 45 (1997) 4713.
[16] S. Zaefferer, N. Chen, Solid State Phenomena 29 (2005) 105.